



1N-26
380733

TECHNICAL MEMORANDUM

X - 55

EXPERIMENTAL INVESTIGATION OF SEVERAL COPPER AND BERYLLIUM
HEMISPHERICAL MODELS IN AIR AT STAGNATION
TEMPERATURES OF 2,000° F TO 3,600° F

By Otto F. Trout, Jr.

Langley Research Center
Langley Field, Va.

NATIONAL AERONAUTICS AND SPACE ADMINISTRATION
WASHINGTON

September 1959
Declassified September 1, 1961

NATIONAL AERONAUTICS AND SPACE ADMINISTRATION

TECHNICAL MEMORANDUM X-55

EXPERIMENTAL INVESTIGATION OF SEVERAL COPPER AND BERYLLIUM

HEMISPHERICAL MODELS IN AIR AT STAGNATION

TEMPERATURES OF 2,000° F TO 3,600° F*

By Otto F. Trout, Jr.

SUMMARY

As part of an investigation by the National Aeronautics and Space Administration to determine the resistance to heating of various materials when used as a heat sink for hypersonic airframes, hemispherical nose-shape models of beryllium and copper have been tested in a Mach number 4 hot-air jet at stagnation temperatures of 2,000° F to 3,600° F and Reynolds numbers of 1.88×10^6 to 2.93×10^6 . The experimental results of heating on the nose of the beryllium models agreed reasonably well with theoretical results, whereas heating on the nose of the copper models was almost twice that predicted by theory. Heating of the cylindrical wall behind the hemisphere agreed fairly well with that predicted by theory at lower temperatures. Beryllium produced a thin protective oxide when heated to its melting point with no tendency to ignite before melting. Copper produced a somewhat heavier layer of oxide upon heating, and ignited when heated to near its melting point. These tests indicate that beryllium is superior to copper as a heat-sink material because it absorbs more heat per unit weight, has greater resistance to oxidation in heated air, and does not ignite when heated in air up to its melting temperature.

INTRODUCTION

The reentry of ballistic missiles into the atmosphere produces extremely high heating rates on the missile surface. One of the methods suggested for alleviating the effects of these high heating rates is the absorption of heat into a material having a high heat capacity. The use of heat-sink materials offers the advantage of simplicity but adds the penalty of additional weight to the missile airframe; therefore, it is necessary to choose a material which will absorb the greatest amount of

*Title, Unclassified.

heat per unit weight and retain sufficient strength to support the loads imposed on it.

Some of the other material properties which must be considered are the rate of oxidation and ignition of the material in high-temperature air. (See ref. 1.) Oxidation can add heat to the model and cause loss of material. Ignition of many of the metals takes place at temperatures considerably below their melting points. When ignition takes place the entire model may be destroyed or consumed at a rate several times that produced by aerodynamic heating, because of the additional heat and the mass loss due to rapid oxidation.

Beryllium and copper have been suggested because of their high heat-capacity-to-weight ratio as compared with other available metals. Copper is readily available as a material of construction and is easily formed by conventional methods, but has the disadvantage of high density and low strength. Beryllium has a higher heat capacity per unit weight, lower density, and higher strength per unit weight than copper; however, beryllium is not readily available and is difficult to fabricate.

Beryllium and copper have been considered by a number of authors as aircraft structural materials suitable for absorption of heat as indicated by references 2 and 3. Exploratory tests of copper and beryllium in a high-temperature airstream are reported in references 4, 5, and 6.

As a part of NASA research on materials to withstand aerodynamic heating, models of commercially pure beryllium and copper have been tested in the pilot model ceramic-heated air jet at the Langley Research Center to observe the reaction of these materials in high-temperature air and make some measurements of the aerodynamic heating associated therewith. The results of the tests, a comparison with calculated heating for the models, and a description of the testing apparatus are presented in the present paper.

SYMBOLS

c_p	specific heat of air at constant pressure, Btu/lb/°F
c_w	specific heat of wall, Btu/lb/°F
D	diameter, ft
h	local aerodynamic heat-transfer coefficient, Btu/(sec)(sq ft)(°F)

k	thermal conductivity of air, Btu/(sec)(sq ft)(°F/ft)
M	Mach number
N_{Pr}	Prandtl number, $c_p\mu/k$
N_{Re}	Reynolds number
p_t	stagnation pressure, psia
t_w	wall thickness, ft
T	absolute temperature, °R
T_{aw}	adiabatic-wall temperature, °R
T_t	stagnation temperature, °F unless otherwise stated
T_w	wall temperature, °R
V	velocity, ft/sec
β	velocity gradient along surface near stagnation point
μ	absolute viscosity of air, lb-sec/sq ft
ρ_w	mass density of wall, lb/cu ft
τ	time, sec

APPARATUS

The present series of tests were conducted in the pilot model ceramic-heated air jet at the Langley Research Center, a photograph of which is presented in figure 1. A diagram of the construction of this facility is presented in figure 2. This unit consists of a ceramic-pebble-bed heat exchanger contained in a pressure tank, attached to an $M = 4$ supersonic nozzle with a 4.0-inch-diameter exit exhausting to the atmosphere.

The pebble bed consists of 3/8-inch-diameter zirconia spheres randomly packed into a bed 28 inches in diameter and approximately 14 feet high, supported by a 6-foot-high bed of 3/8-inch-diameter alumina spheres.

The pebble bed is surrounded by various types of brick that are placed in such a manner as to insulate the pebble bed, insulate the pressure tank, and prevent bypass flow. The brickwork is laid up with the joints of the various layers staggered, with all the voids filled with cement, and all the bricks tightly fitted together to prevent air from flowing through the brickwork and thus bypassing the pebble bed.

In preparation for a test, the ceramic bed is heated by a propane-air-oxygen burner (fig. 2) by pressure firing down through the pebble bed and exhausting out of the bottom of the pressure vessel. Some of the products of combustion are also allowed to pass through the nozzle to heat the brickwork leading to the nozzle. When the ceramics are heated to the desired temperature, the burner is closed off and air is brought in through the bottom of the bed, heated while passing through the pebble bed, and discharged through the nozzle exit.

Figure 3 presents a photograph of a model in the test section of the ceramic-heated air jet. The model is mounted on a water-cooled, movable arm which swings the model into the jet by remote control when the desired flow is established in the nozzle. The model can be removed from the jet at any time during the test at the control of the operator.

Thermocouple and pressure data from both the model mounted in the jet and related jet equipment are recorded on an oscillograph. Reactions of the model during tests are observed visually and recorded by high-speed motion-picture cameras. Shadowgraph data are also recorded by a motion-picture camera.

Figure 4 presents jet properties for the $M = 4$ nozzle operating at a stagnation pressure of 815 psia and at stagnation temperatures from $2,000^{\circ}\text{F}$ to $4,000^{\circ}\text{F}$. Figure 4(a) presents the variation of Mach number and velocity with stagnation temperature. The decrease in Mach number with increasing temperature is due to the decrease in specific heat ratio. Figure 4(b) presents free-stream pressure and temperature plotted against stagnation temperature for the free jet. Figure 4(c) presents the calculated values of Reynolds number per foot plotted against stagnation temperature.

Figure 4(d) presents heating rate on the stagnation point of a hemispherical model for the present facility as calculated by methods presented in references 7 and 8:

$$h\sqrt{D} = 0.763N_{Pr}^{0.4} \sqrt{\frac{3D}{V}} \sqrt{N_{Re}} k$$

where D is the model diameter, and the physical properties and flow velocity of air are evaluated immediately behind the normal shock. The

jet properties presented in figure 4 were calculated from equations presented in reference 7, with the average value of the specific heat ratio for air being used when calculating the change in conditions accompanied by change in free-stream pressure.

MODELS AND TESTS

The present series of tests consists of heating a series of three copper and three beryllium models in the ceramic-heated air jet. Figure 5 presents a diagram showing pertinent details of each of the three sizes of models tested. Two models of each size were constructed - one of beryllium and the other of copper. The 1-inch-diameter hemispherical models consisted of a hemisphere supported by a cylinder of the same material. Wall thickness was held constant at 0.125 inch. Thermocouples were installed by spot welding them in the models at the stagnation point, at 40° from the stagnation point, and approximately 1/2 inch behind the intersection of the hemisphere and cylinder as shown in figure 5. The 3/4-inch-diameter models were identical to the 1-inch-diameter models except for the diameter. The 3/8-inch-diameter hemispherical models were constructed with a 0.094-inch-thick wall. The only thermocouple in this model was placed at the stagnation point.

Each model was used for three successive tests. Before each test, the models were polished to a clean, smooth finish. The first two tests were made at stagnation temperatures of $2,000^\circ$ F and $2,900^\circ$ F for 3 seconds each. The third test was made at a stagnation temperature of $3,600^\circ$ F for 10 seconds or until the model ablated. Thermocouple outputs were recorded as a function of time on an oscillograph. The reactions of the models were recorded by high-speed motion-picture cameras and shadowgraphs.

RESULTS AND DISCUSSION

Visual Observations

Figure 6 presents photographs of the 1-inch-diameter beryllium and copper models at various times during the tests and figure 7 presents shadowgraphs of the free jet and the three model sizes during typical tests.

Upon being heated, beryllium formed a thin, smooth protective oxide which did not appear to increase in thickness with time or temperature. Near the melting point, the soft beryllium was blown from the model, but had no tendency to ignite. Visual observation of the models after the tests showed that they did not spall or crack from thermal shock caused by rapid heating.

Copper, as compared with beryllium, formed a thicker oxide on the surface. Near the melting point, the copper ignited and burned rapidly. Because copper was relatively soft, foreign particles from the jet caused indentations in the surface. Copper also showed no tendency to spall or crack from rapid heating.

Calculation of Heating on Models

Heating on the stagnation point and the 40° point on the hemisphere of the models was calculated by methods presented in reference 8, whereas heating on the cylinder behind the hemisphere was calculated by methods presented in reference 9, with the values of specific heats for beryllium and copper as presented in references 10 and 11 being used. (See fig. 8.) Rate of change of the temperature of the model wall may be expressed as follows:

$$dT_w = \frac{(T_{aw} - T_w)h}{\rho_w c_w t_w} d\tau$$

In the calculations, the values of mass density used were 115 lb/cu ft for beryllium and 559 lb/cu ft for copper. The following assumptions were made in the calculation of wall heating: constant temperature through the wall, no transport of heat due to conduction parallel with the wall, and no loss of heat due to radiation.

Heating on the 3/8-inch-diameter model was also calculated for the total hemisphere from the relation

$$h_s = 0.5h_{stag}$$

where h_s is the heat-transfer coefficient on the total frontal area of the hemisphere and h_{stag} is the heat-transfer coefficient at the stagnation point.

Experimental and Calculated Heating on Beryllium Models

Figure 9 presents the experimental and calculated heating data for the 1-inch-diameter hemispherical beryllium model at stagnation temperatures of $2,000^\circ$ F, $2,900^\circ$ F, and $3,600^\circ$ F. Heating at the stagnation point and the 40° point of the hemisphere is slightly above that predicted by theory in the earlier part of the tests, whereas it is, in general, less than that predicted in the later part of the tests. Heating

in the earlier part of the tests more closely approximates theoretical assumption of aerodynamic heating since radiation and conduction effects are the least at this time. Both radiation and conduction would tend to lower the stagnation-point temperature at the later part of the test. Heating of the cylinder behind the hemisphere agrees with theoretical predictions in the 2,000° F test (fig. 9), but is less than that predicted as stagnation temperature is increased, probably because of the increased absorption of heat from the boundary layer by the hemisphere ahead of the cylinder as stagnation temperature is increased.

Figure 10 presents the heating data for the 3/4-inch-diameter hemispherical beryllium model. Heating on the hemisphere is higher than that predicted by theory in the early part of the test. Heating on the cylinder behind the hemisphere follows the same pattern as that of the 1-inch-diameter beryllium model.

Figure 11 presents the experimental heating data for the stagnation point of the 3/8-inch-diameter beryllium hemispherical model and compares these data with those obtained from theory for heating on the stagnation point and on the total hemisphere. Inasmuch as the model is small with relatively thick walls, the experimental values of heating do not approximate those predicted by theory since conduction and radiation are not taken into account.

Experimental and Calculated Heating on Copper Models and Comparison With Beryllium Models

Figure 12 presents the experimental and calculated heating data for the 1-inch-diameter copper hemispherical model for heating on the stagnation point, the 40° point, and the cylinder behind the hemisphere. Initial heating on the stagnation point and the 40° point is considerably greater than that predicted by theory for laminar flow on the surface. Because of the high heat conduction of copper, the cylinder behind the hemisphere heated more rapidly than predicted by theory after the initial part of the test. As stagnation temperature is increased, the increase of heating rate on the cylinder is less than predicted by theory and the trends are similar to those for the beryllium models in the initial part of the tests.

Figure 13 presents the heating data for the 3/4-inch-diameter copper hemispherical models. The trends observed here are similar to those of the 1-inch-diameter copper models.

Figure 14 presents the experimental and calculated heating data for the 3/8-inch-diameter copper hemispherical models. Because of the relatively thick wall, as compared with the diameter of model, and the high

thermal conductivity of copper, simple theory does not predict the heating when conduction and radiation are not taken into account. A comparison of the heating of the 3/8-inch-diameter copper model (fig. 14) and the 3/8-inch-diameter beryllium model (fig. 11) indicates that the copper models are heated at a higher rate than predicted by theory.

Oxidation may be an important factor on the heating rate even if the depth of oxidation is less than 1 mil. The oxidation of beryllium to beryllium oxide produces 27,150 Btu/lb of beryllium, whereas the oxidation of copper to cupric oxide produces 9,880 Btu/lb of copper or 5,760 Btu/lb of copper if the cuprous oxide is formed. The temperature rise per mil of surface depth oxidized is

$$\Delta T = \frac{qt_m}{t_w c_w}$$

where

q heat formation of oxide per pound of metal oxidized, Btu/lb

t_m thickness of metal oxidized, ft

t_w thickness of wall of flat plate, ft

c_w heat capacity of metal wall, Btu/lb/°F

Therefore, for a flat plate 0.125 inch thick, the oxidation of a layer 0.001 inch thick will increase the wall temperature 434° F for beryllium and 880° F for copper if the cupric oxide is formed or 513° F if the cuprous oxide is formed and all of the heat of oxidation is absorbed into the parent metal.

Since copper turns color immediately upon entering the hot airstream because of the oxidation on the surface, the model will be heated from the oxidation process as well as from the aerodynamic heating process. Because the models were polished to the bare metal surface before they were tested, the high heating rates on the copper models, at the initial part of the test, may possibly be due to oxidation of the polished surface. Some of the heat rise on the beryllium models may be due to oxidation, although the effect is not so large as for copper.

Corrections for radiation were not made on the theoretical heating of the models because no values of emissivity were available over the temperature range the models were heated.

CONCLUSIONS

The results obtained from tests of copper and beryllium hemispherical models in a Mach number 4 hot-air jet at stagnation temperatures of 2,000° F to 3,600° F indicated the following:

1. Upon being heated, beryllium forms a thin, smooth protective oxide which does not thicken appreciably with increasing temperature and exhibits no tendency to ignite below its melting point. Soft beryllium blows away near its melting point. Copper, as compared with beryllium, forms a somewhat heavier oxide layer before reaching its melting point and exhibits a tendency to burn rapidly.
2. Qualitative heat-transfer measurements on copper and beryllium models tested under identical conditions show a trend of higher heating rates for the copper than for the beryllium. Heating on the hemispherical nose of the beryllium models is slightly above that predicted by theory whereas heating on the nose of the copper models is considerably higher than that predicted by theory. Heating on the cylinder behind the hemisphere shows a trend of becoming less than that predicted by theory as stagnation temperature is increased.
3. Calculation of the heating produced by oxidation of the surface, even for moderate depths, shows that oxidation may possibly be a significant factor in raising the temperature of a thin wall.

Langley Research Center,
National Aeronautics and Space Administration,
Langley Field, Va., May 15, 1959.

REFERENCES

1. Grobecker, D. W., ed.: Metals for Supersonic Aircraft and Missiles. A.S.M. (Cleveland, Ohio), c.1958.
2. Micks, W. R., and Hoffman, G. A.: A Re-Evaluation of Beryllium as a Potential Structural Material for Use in Flight Vehicles. U. S. Air Force Project RAND Res. Memo. RM-1642, The RAND Corp., May 7, 1956.
3. Foster, R. E., and Riedinger, L. A.: Future Weight Reductions With Beryllium. LMSD-2526 (S.A.W.E. Paper 159), Lockheed Aircraft Corp., Apr. 15, 1957.
4. Purser, Paul E., and Hopko, Russell, N.: Exploratory Materials and Missile-Nose-Shape Tests in a 4,000° F Supersonic Air Jet. NACA RM L56J09, 1956.
5. Kinard, William H.: The Behavior of Beryllium and Beryllium Copper in a 4,000° F Supersonic Air Jet at a Mach Number of 2. NACA RM L57G31, 1957.
6. Fields, E. M., Hopko, Russell N., Swain, Robert L., and Trout, Otto F., Jr.: Behavior of Some Materials and Shapes in Supersonic Free Jets at Stagnation Temperatures up to 4,210° F, and Descriptions of the Jets. NACA RM L57K26, 1958.
7. Ames Research Staff: Equations, Tables, and Charts for Compressible Flow. NACA Rep. 1135, 1953. (Supersedes NACA TN 1428.)
8. Crawford, Davis H., and McCauley, William D.: Investigation of the Laminar Aerodynamic Heat-Transfer Characteristics of a Hemisphere-Cylinder in the Langley 11-Inch Hypersonic Tunnel at Mach Number 6.8. NACA Rep. 1323, 1957. (Supersedes NACA TN 3706.)
9. Lee, Dorothy B., and Faget, Maxime A.: Charts Adapted From Van Driest's Turbulent Flat-Plate Theory for Determining Values of Turbulent Aerodynamic Friction and Heat-Transfer Coefficients. NACA TN 3811, 1956.
10. Battelle Memorial Institute (under direction of C. R. Tipton, Jr.): Materials - General Properties. AECl-3647, The Reactor Handbook, vol. 3, sec. 1, U. S. Atomic Energy Comm., Feb. 1955.
11. Lyman, Taylor, ed.: Metals Handbook. A.S.M. (Cleveland, Ohio), 1948. (Reprinted 1952.)



L-58-1492
Figure 1.- Photograph of the pilot model ceramic-heated air jet at the
Langley Research Center.

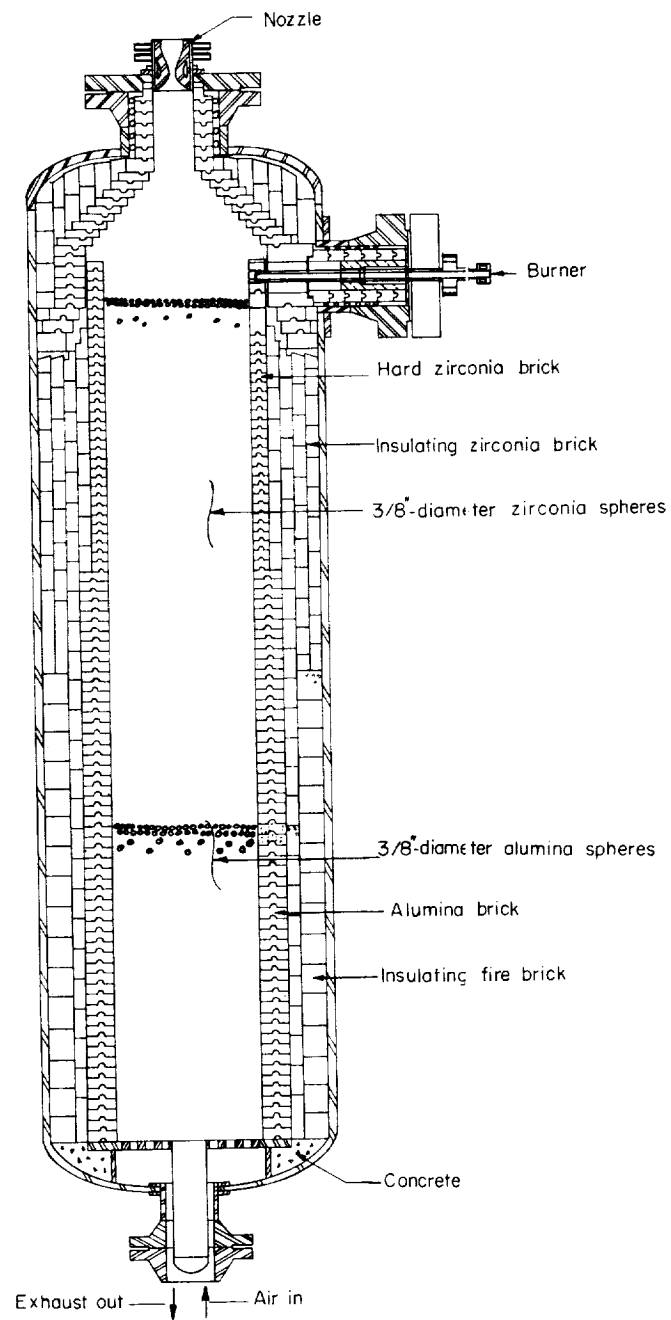
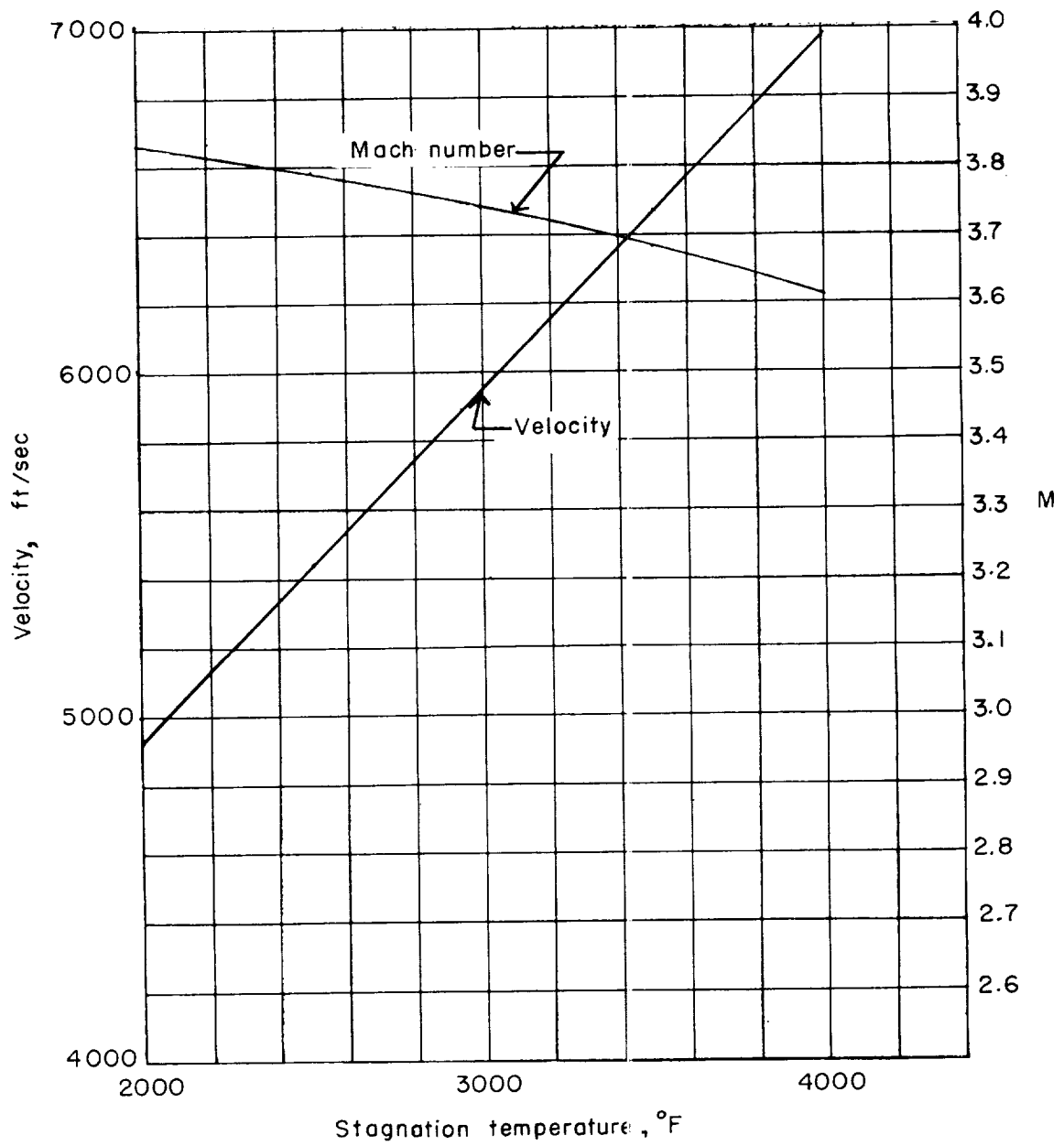


Figure 2.- Diagram of the test facility.

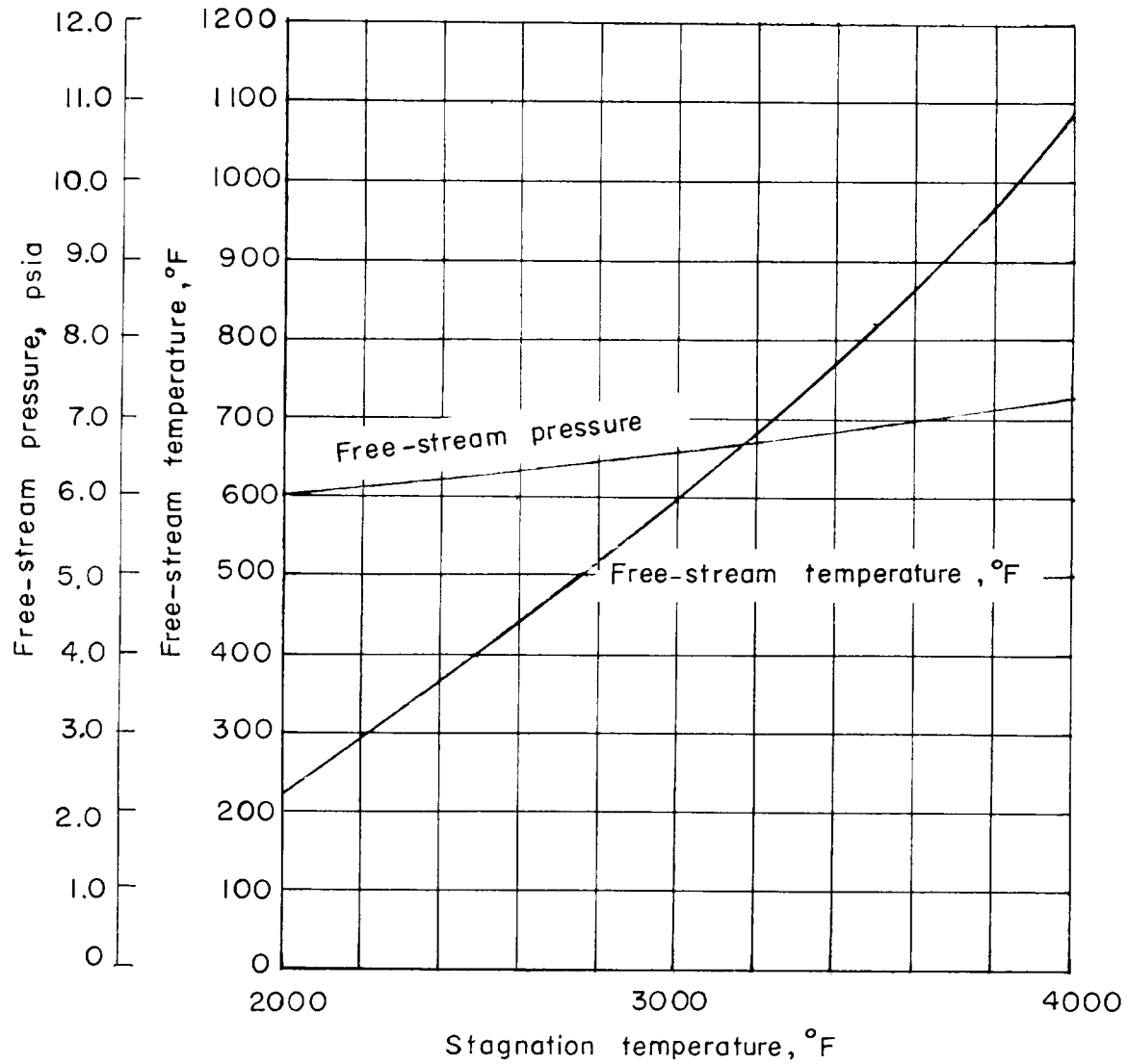


Figure 3.- Photograph of a model in test section. L-58-1491



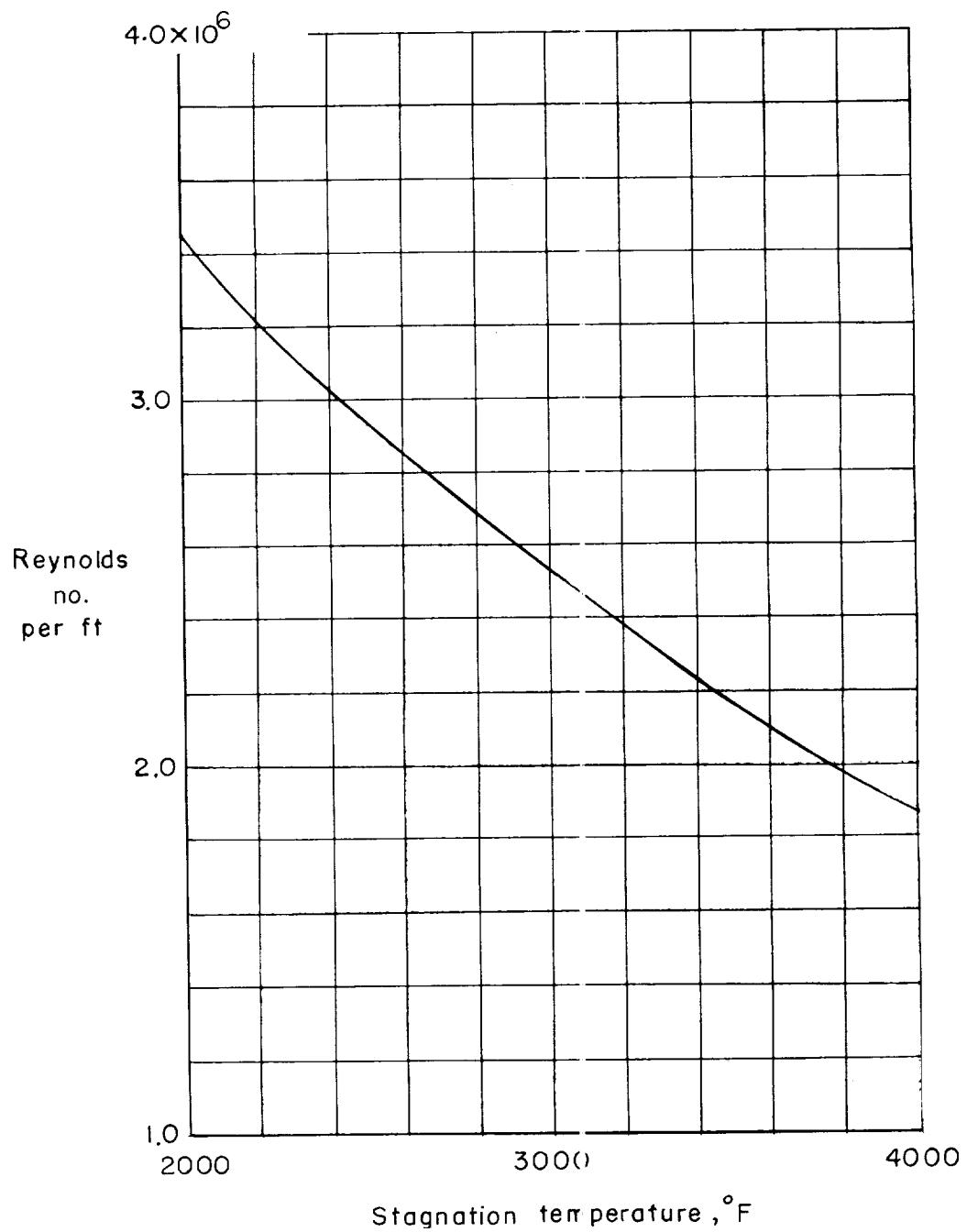
(a) Variation of Mach number and velocity with stagnation temperature.

Figure 4.- Jet properties for the $M = 4$ nozzle operating at a stagnation pressure of 815 psia and at stagnation temperatures from $2,000^{\circ}\text{F}$ to $4,000^{\circ}\text{F}$.



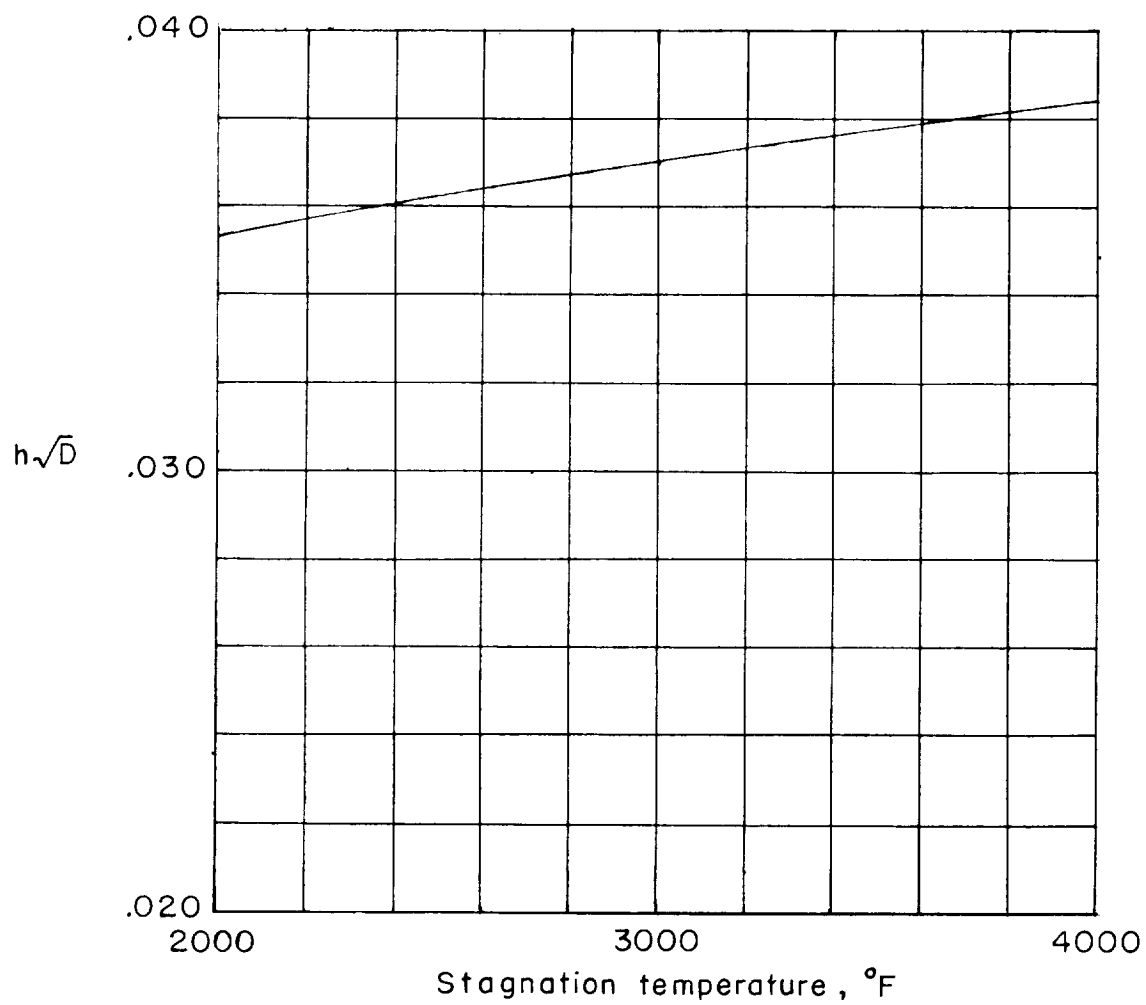
(b) Variation of free-stream pressure and temperature with stagnation temperature.

Figure 4.- Continued.



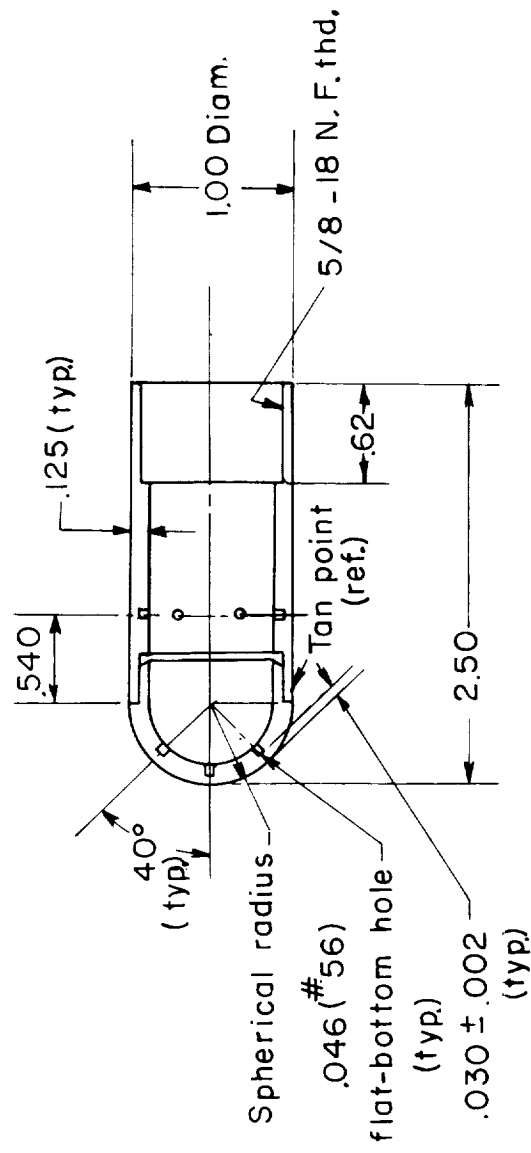
(c) Variation of the calculated values of Reynolds number with stagnation temperature.

Figure 4.- Continued.



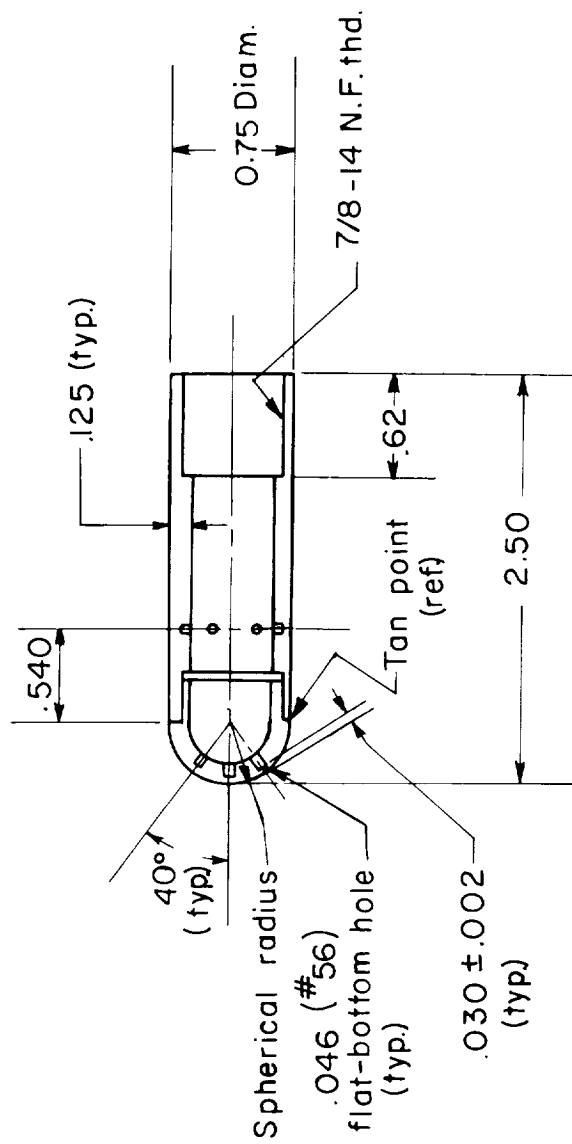
(d) Variation of heating rate for stagnation-point heating of a hemispherical model with stagnation temperature.

Figure 4.- Concluded.



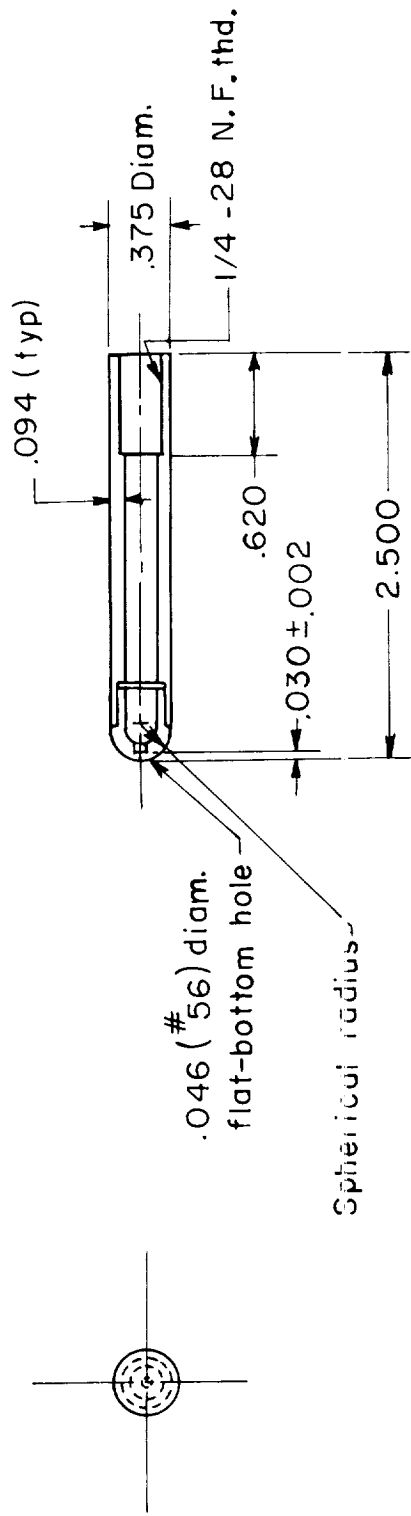
(a) 1-inch-diameter model.

Figure 5.- Pertinent details of models. (All dimensions in inches.)



(b) 3/4-inch-diameter model.

Figure 5.- Continued.

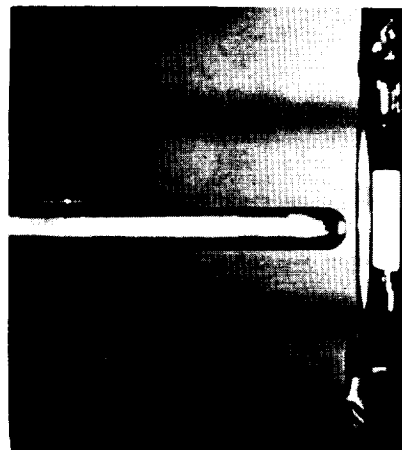


(c) 3/8-inch-diameter model.

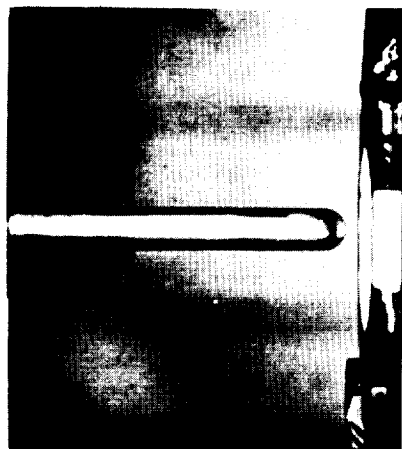
Figure 5.- Concluded.



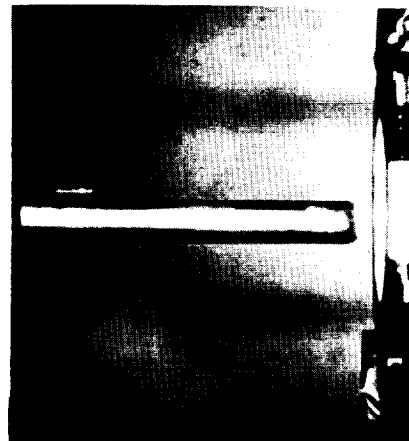
0 Second



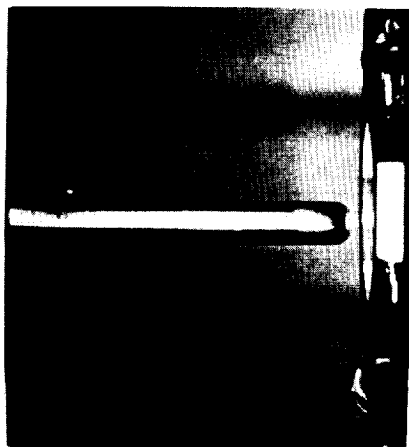
1.0 Second



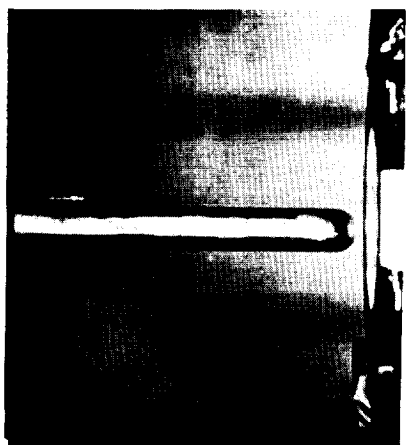
4.0 Seconds



6.0 Seconds



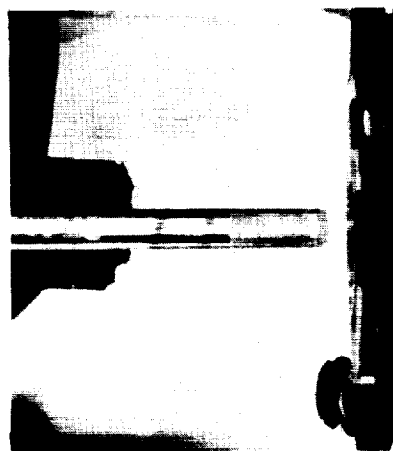
8.0 Seconds



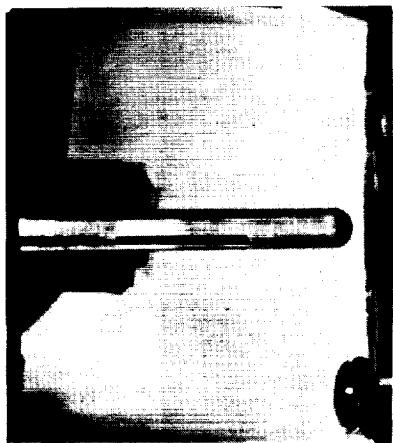
10.0 Seconds

(a) Beryllium model; stagnation temperature, 3,600° F. L-59-3012

Figure 6.- Photographs of the 1-inch-diameter models during test.

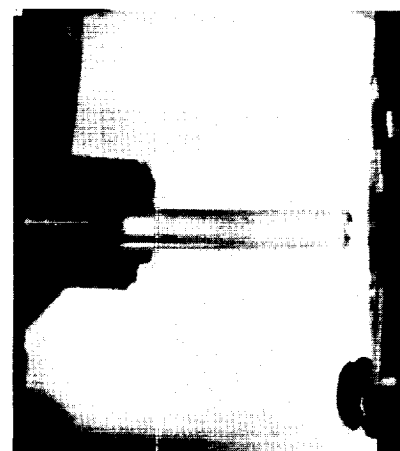
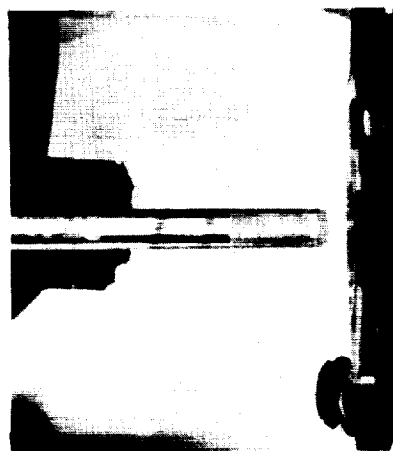


0 Second

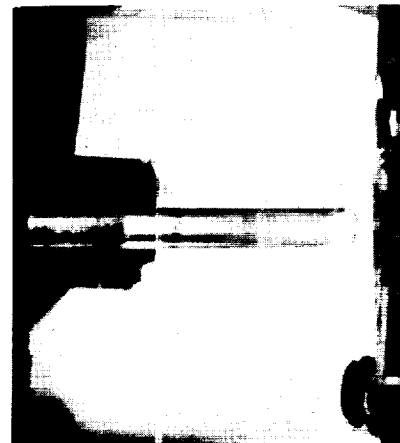


1.0 Second

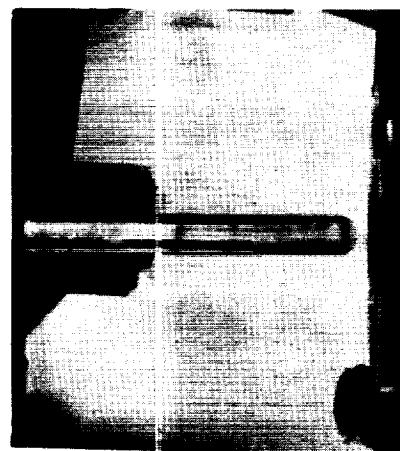
3.0 Seconds



4.0 Seconds



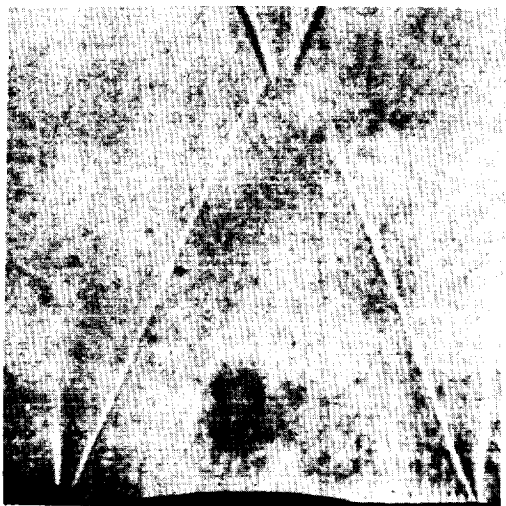
3.6 Seconds



3.1 Seconds

(b) Copper model; stagnation temperature, $3,590^{\circ}\text{F}$. L-59-3013

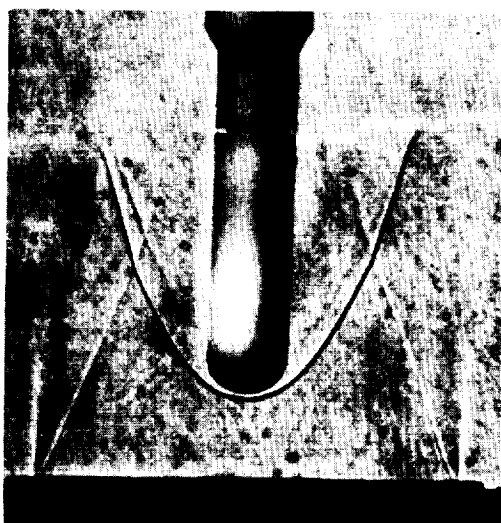
Figure 6.- Concluded.



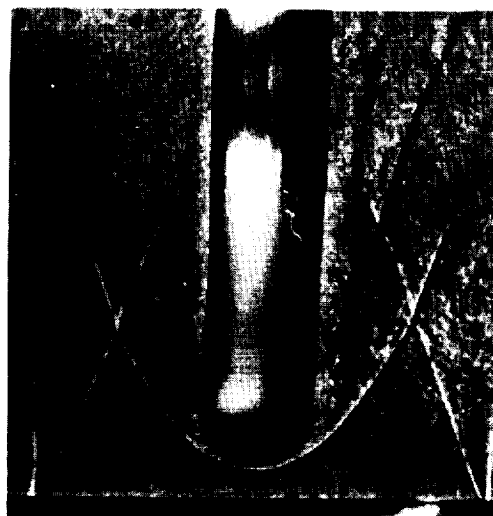
Free jet



3/8 - inch-diameter model



3/4 - inch-diameter model



1 - inch-diameter model

L-59-3014

Figure 7.- Shadowgraphs of tests in free jet of $M = 4$ nozzle. Average stagnation temperature, $3,600^{\circ}\text{F}$; stagnation pressure, 815 psia.

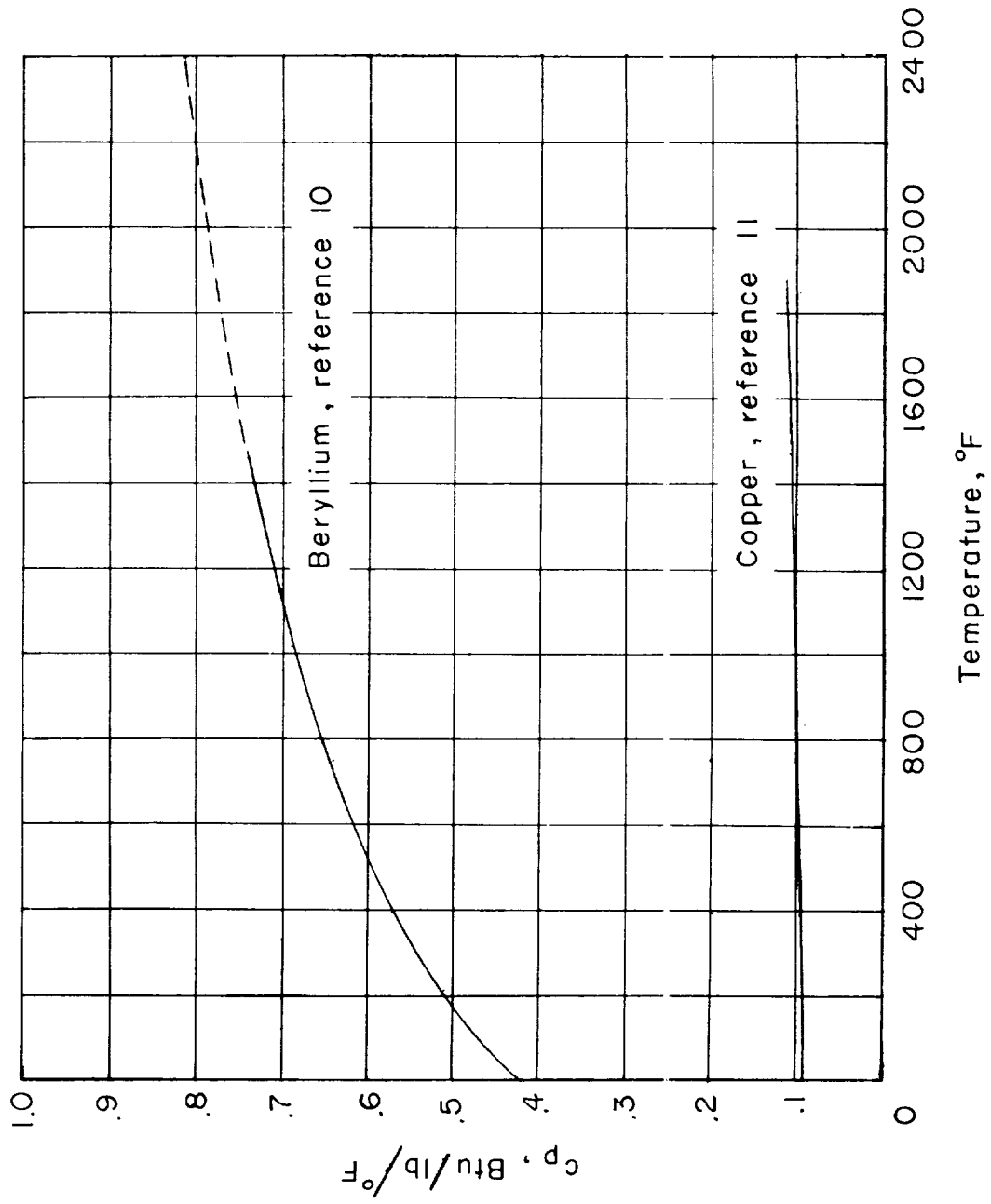
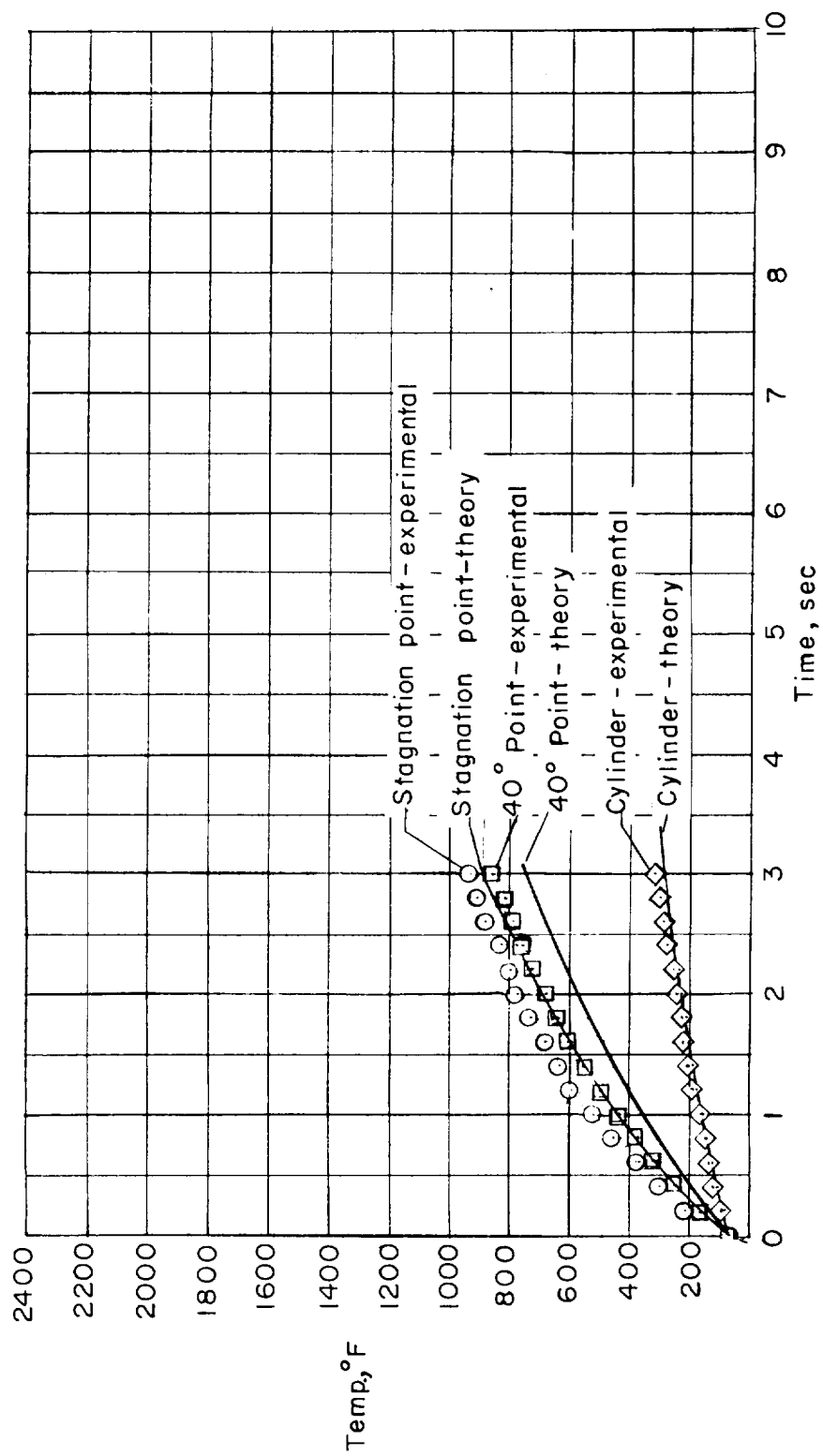
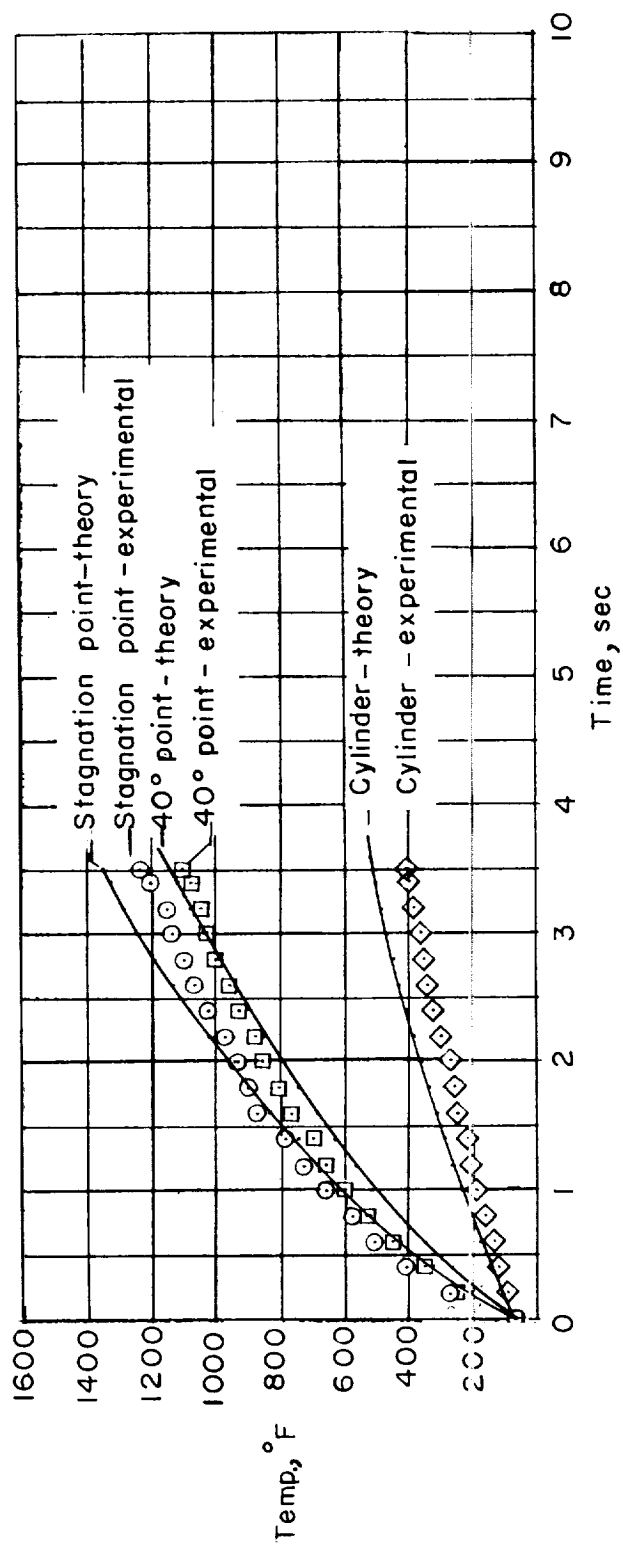


Figure 8.- Specific heat of copper and beryllium plotted against temperature.



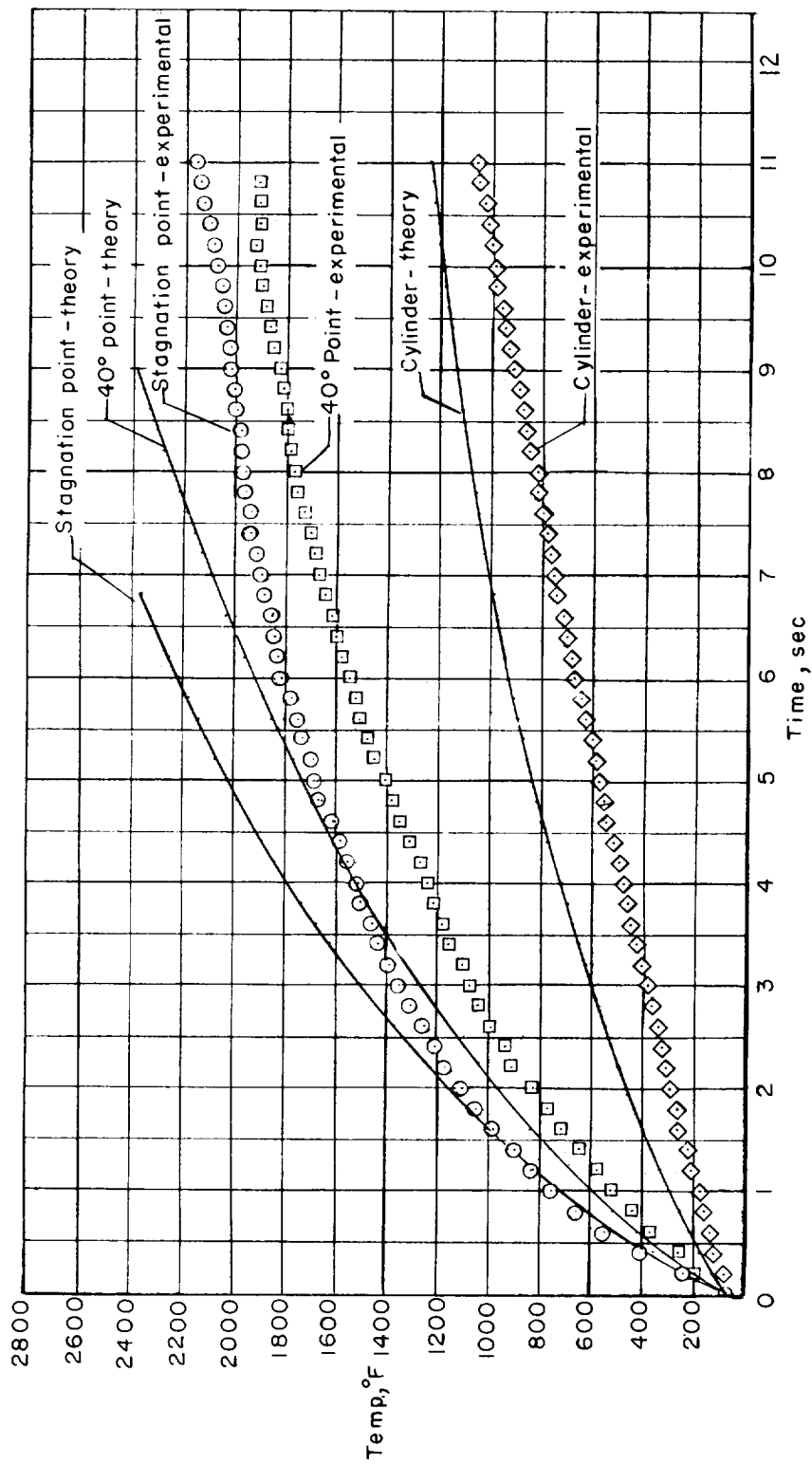
(a) $T_t = 2,000^\circ \text{F}$.

Figure 9.- Heating of the 1-inch-diameter model. $p_t = 815$ psia.



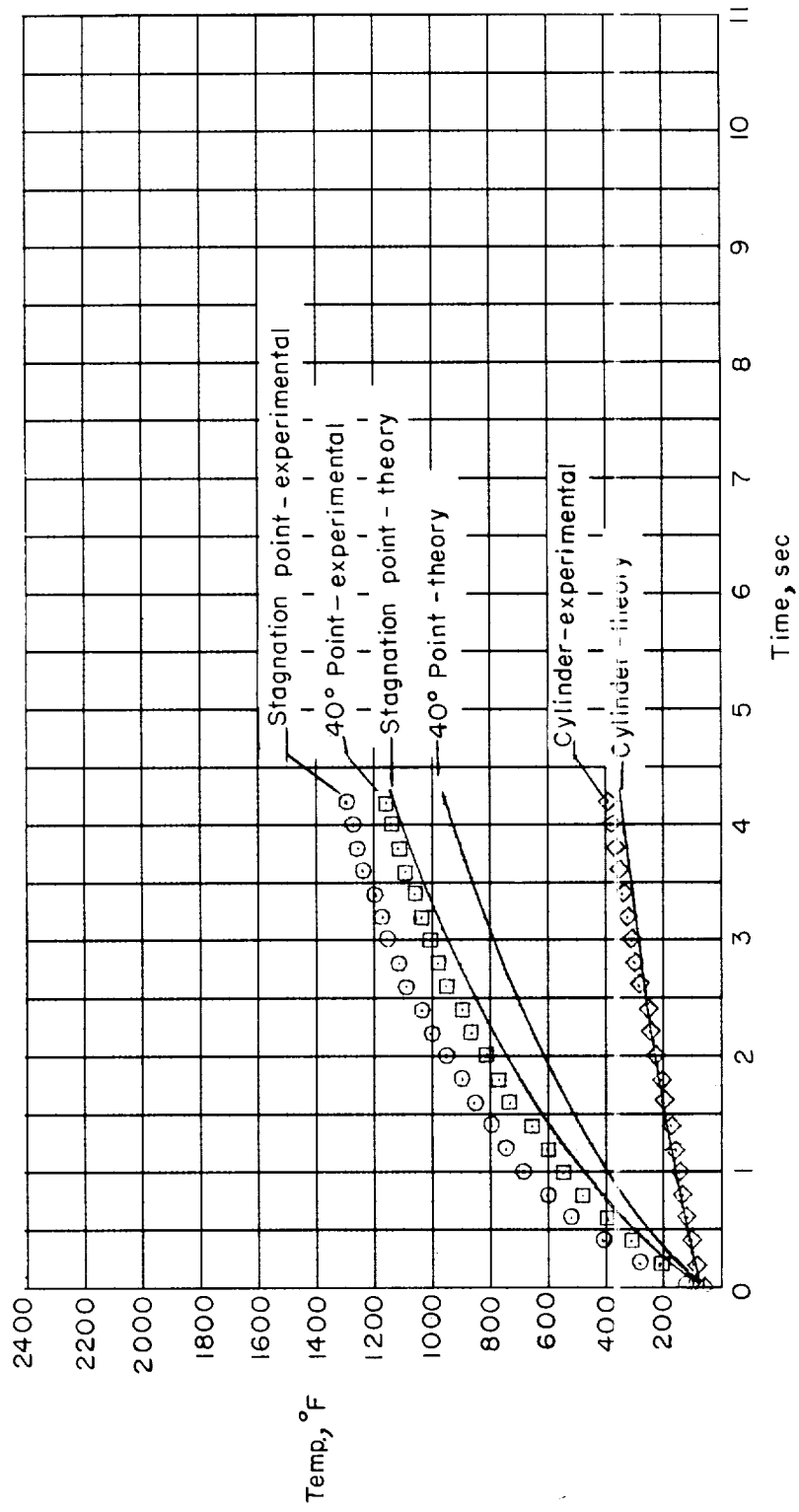
(b) $T_t = 2,900^\circ \text{F}$.

Figure 9.- Continued.



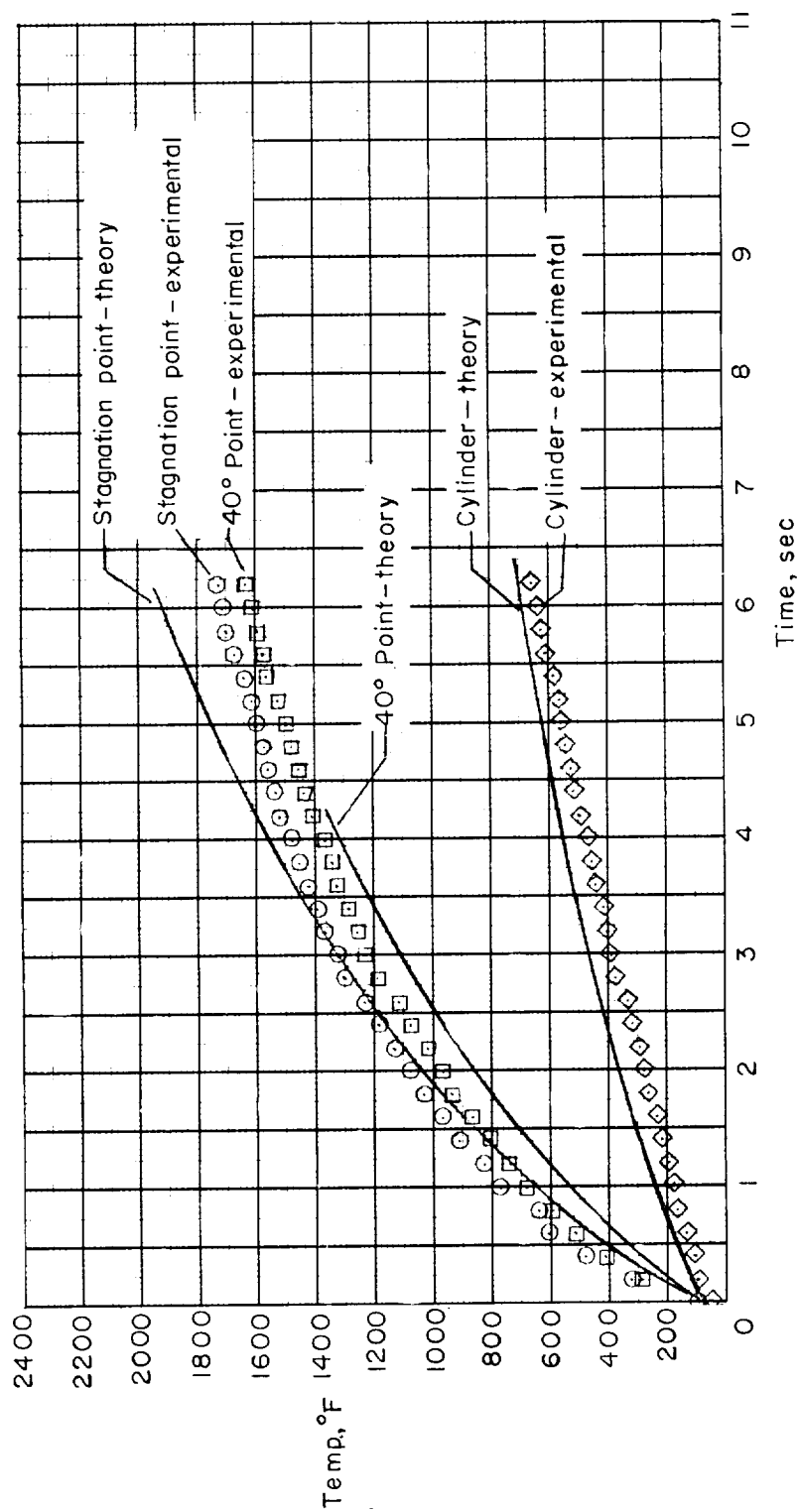
(c) $T_t = 3,600^\circ \text{F}$.

Figure 9.- Concluded.



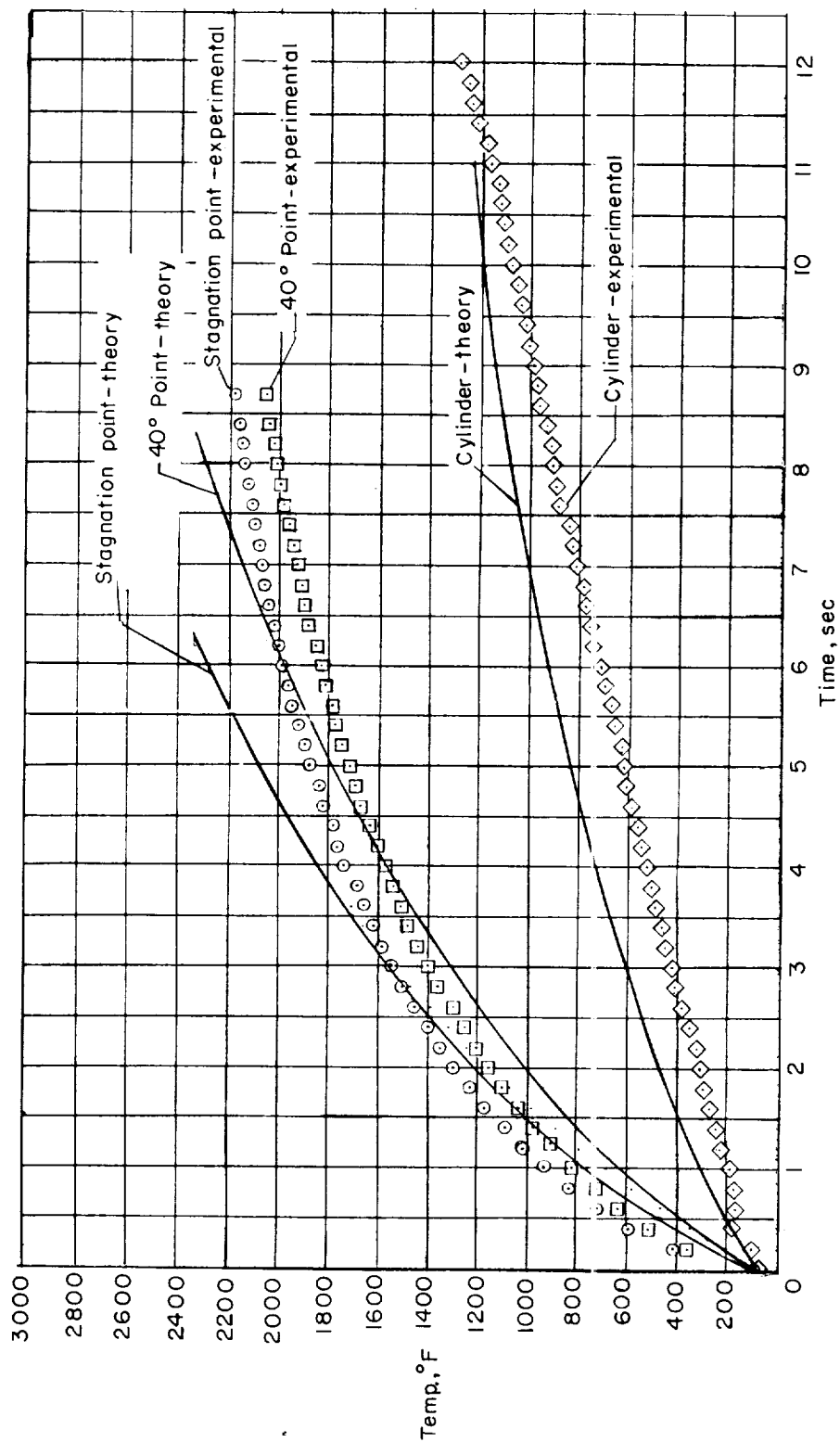
(a) $T_t = 2,000^\circ \text{ F.}$

Figure 10.- Heating of the 3/4-inch-diameter hemispherical beryllium model. $p_t = 815 \text{ psia.}$



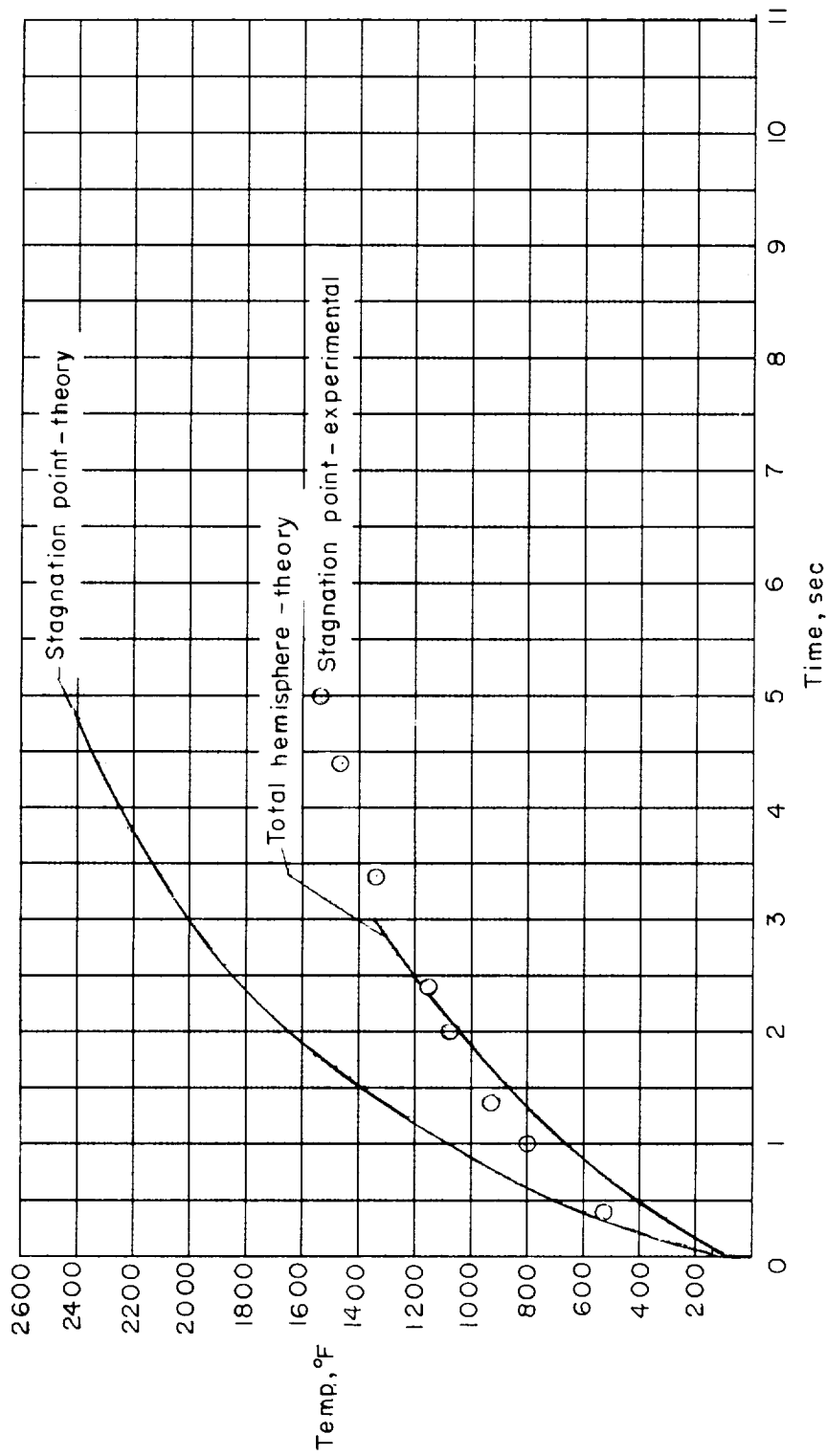
(b) $T_t = 2,900^\circ \text{ F.}$

Figure 10.- Continued.



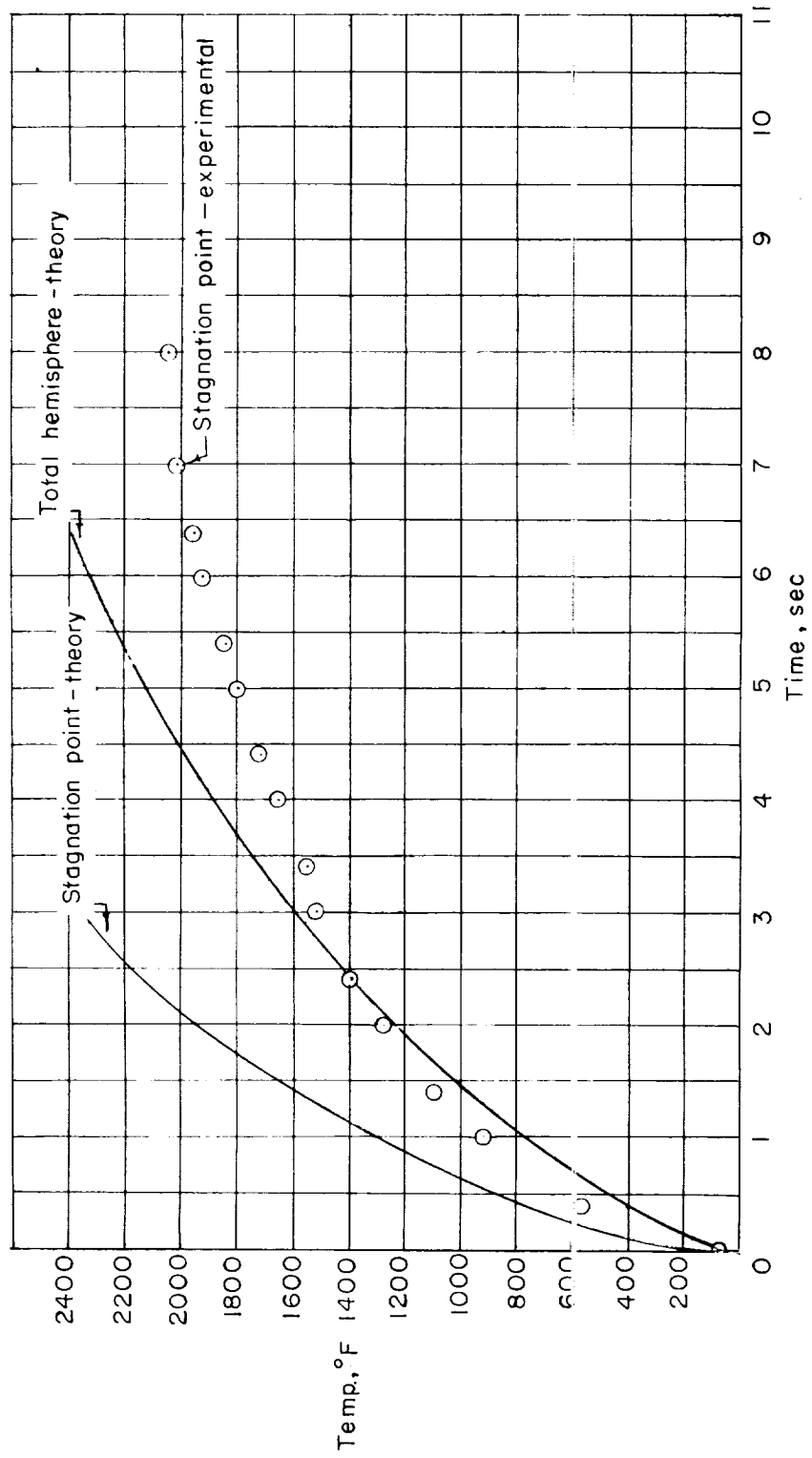
(c) $T_t = 3,600^\circ \text{F}$.

Figure 10.- Concluded.



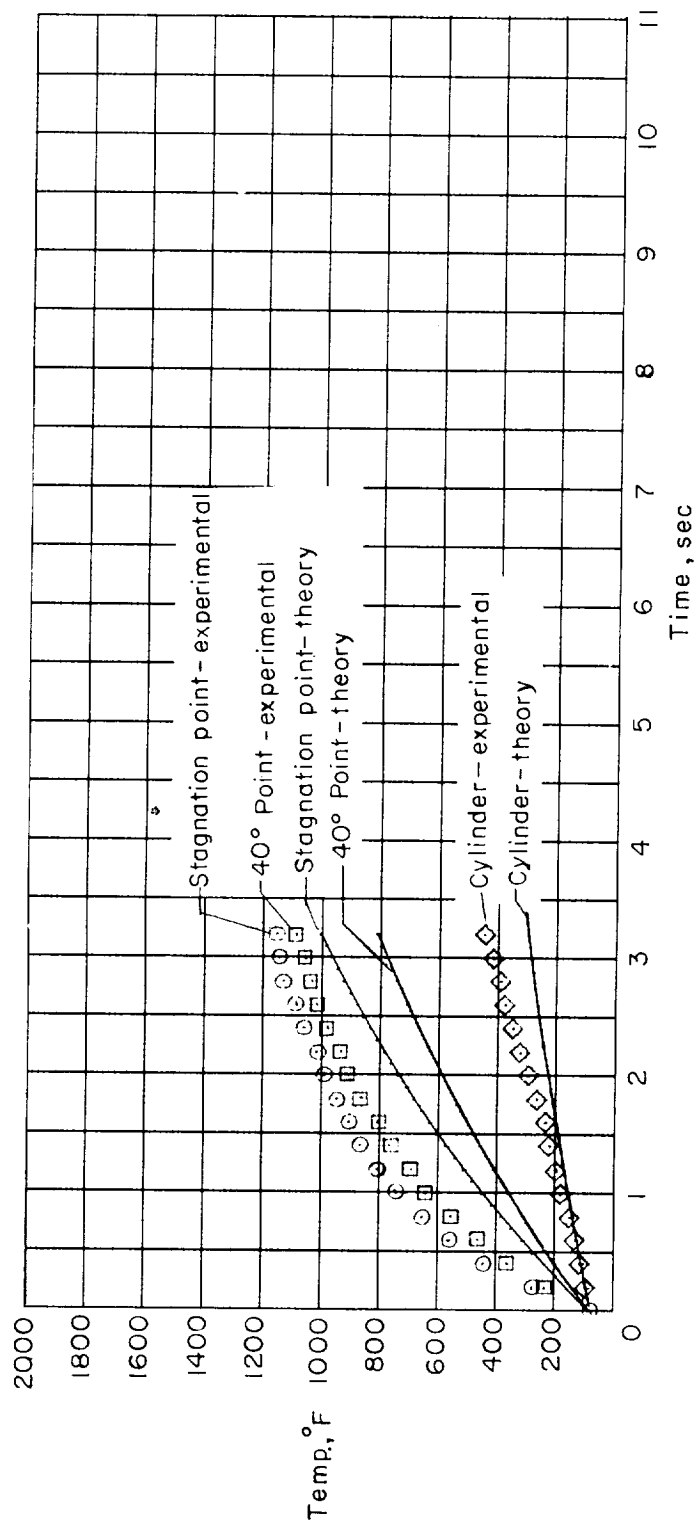
(a) $T_t = 2,900^\circ \text{F}$.

Figure 11.- Heating of the 3/8-inch-diameter hemispherical beryllium model. $p_t = 815 \text{ psia}$.



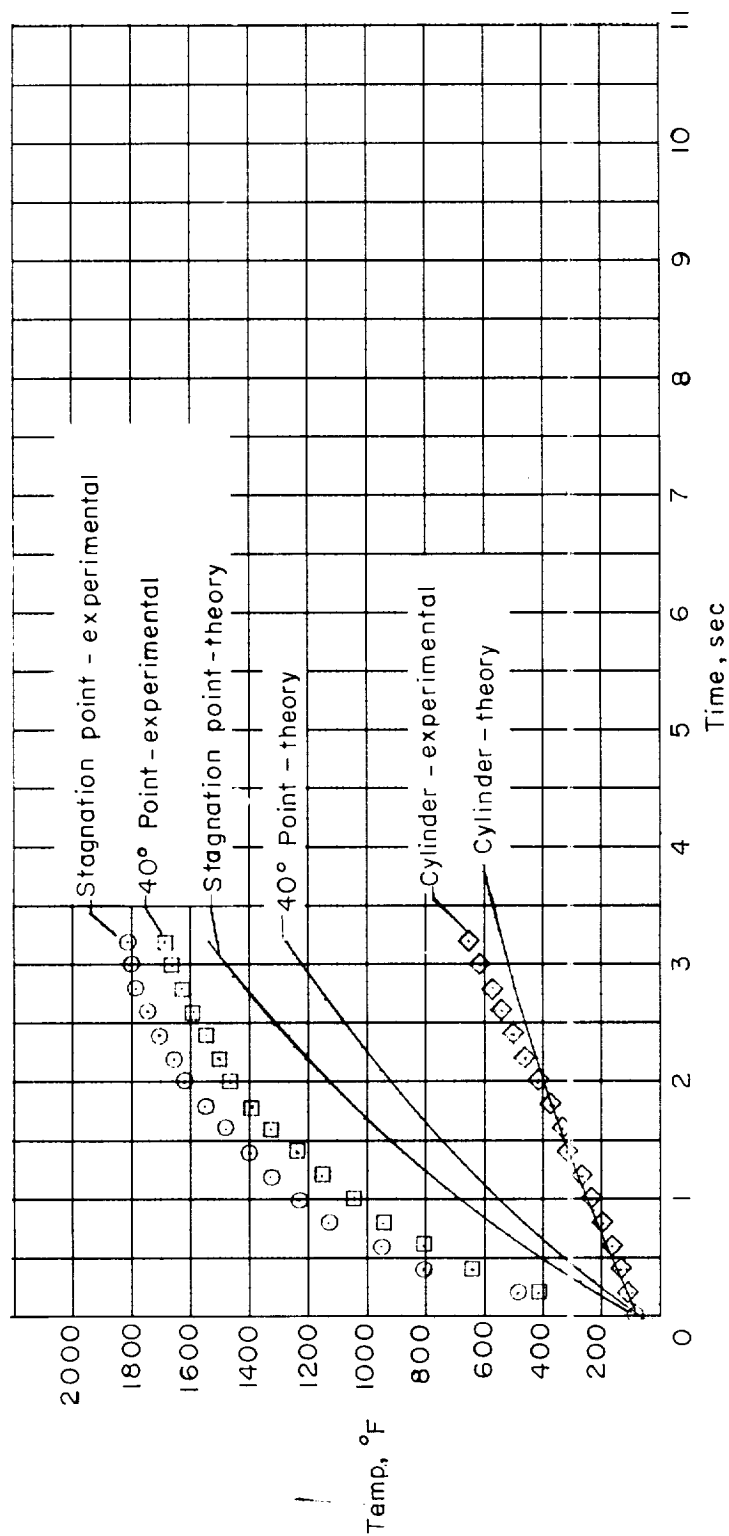
(b) $T_t = 3,575^\circ \text{F.}$

Figure 11.- Concluded.



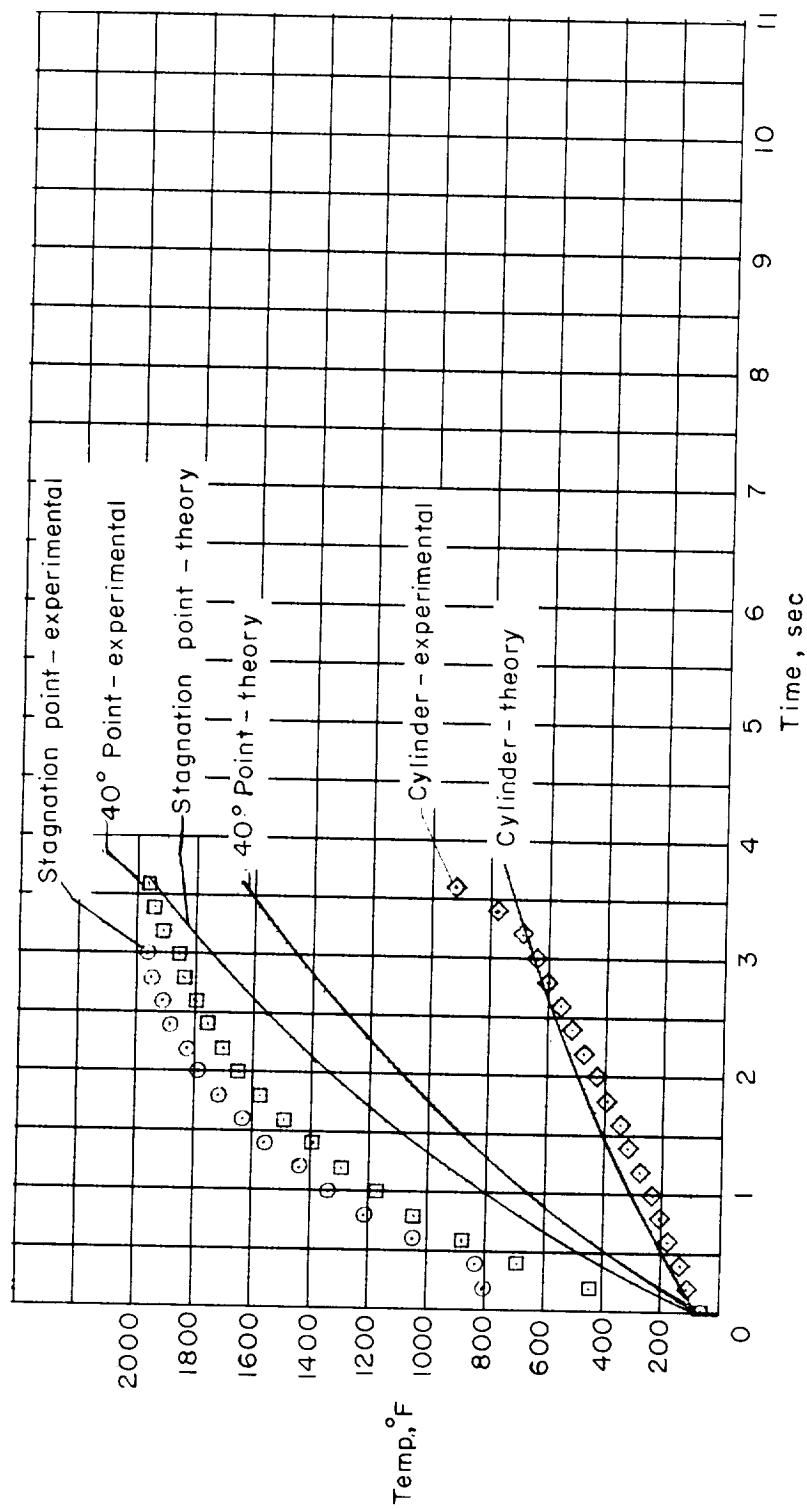
(a) $T_t = 1,960^\circ \text{F.}$

Figure 12.- Heating of the 1-inch-diameter hemispherical copper model. $p_t = 815 \text{ psia.}$



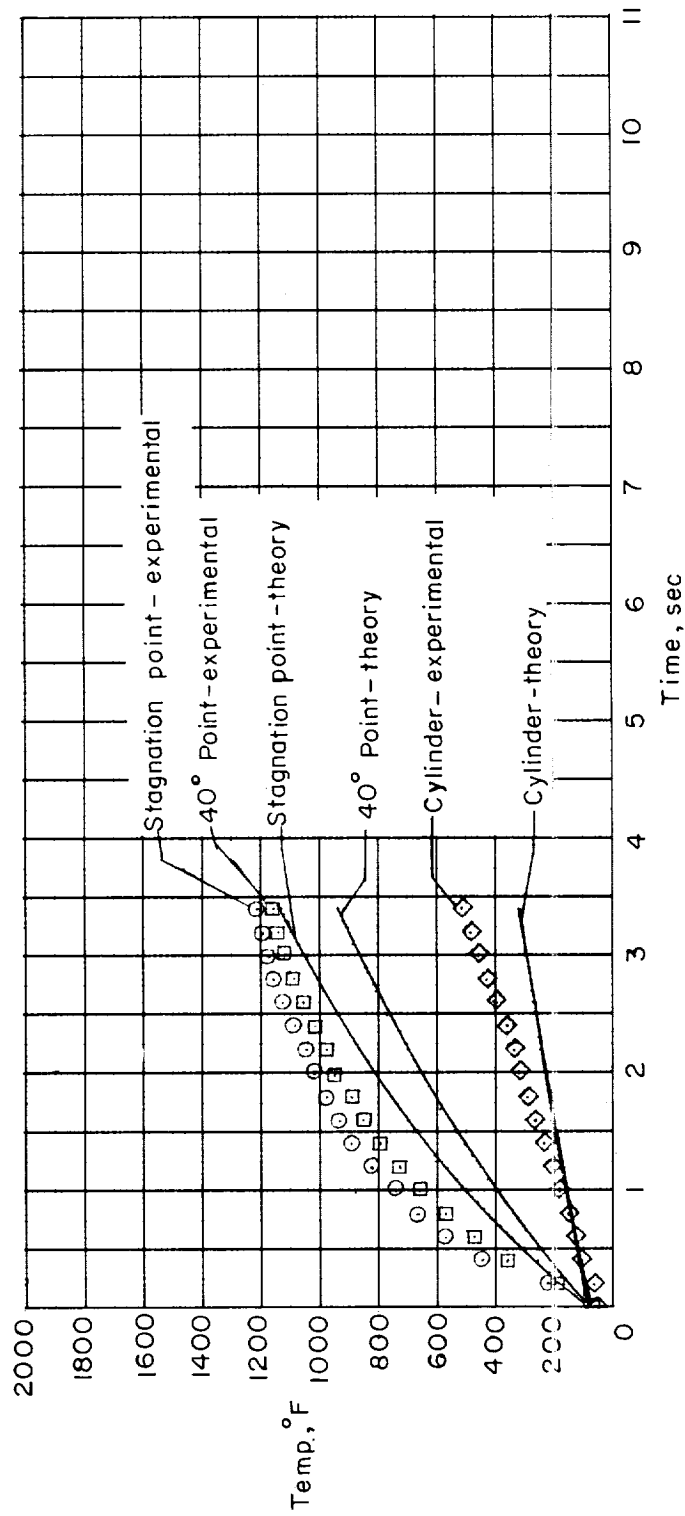
(b) $T_t = 3,010^\circ \text{ F}$.

Figure 12.- Continued.



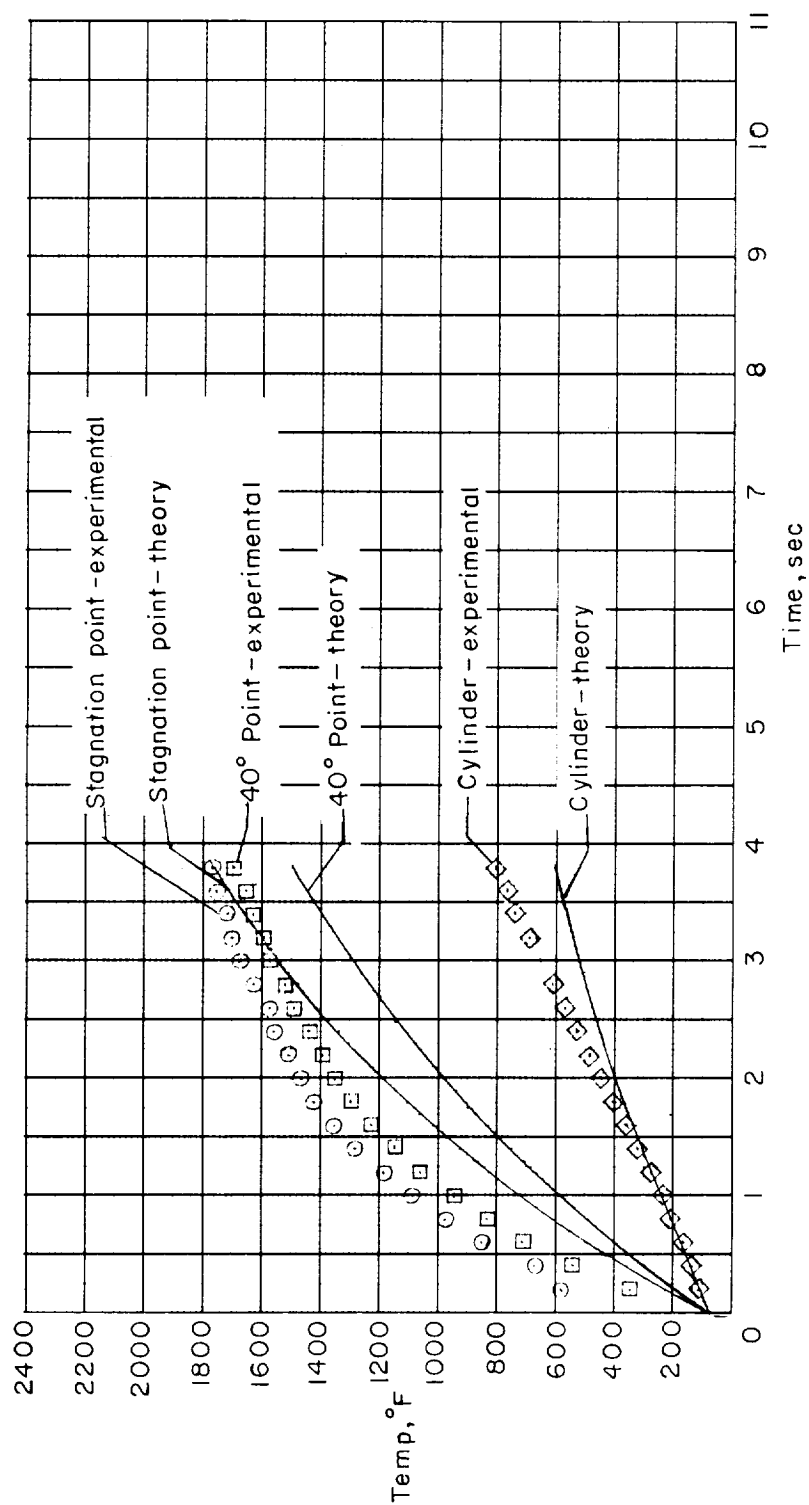
(c) $T_t = 3,590^\circ \text{ F.}$

Figure 12.- Concluded.



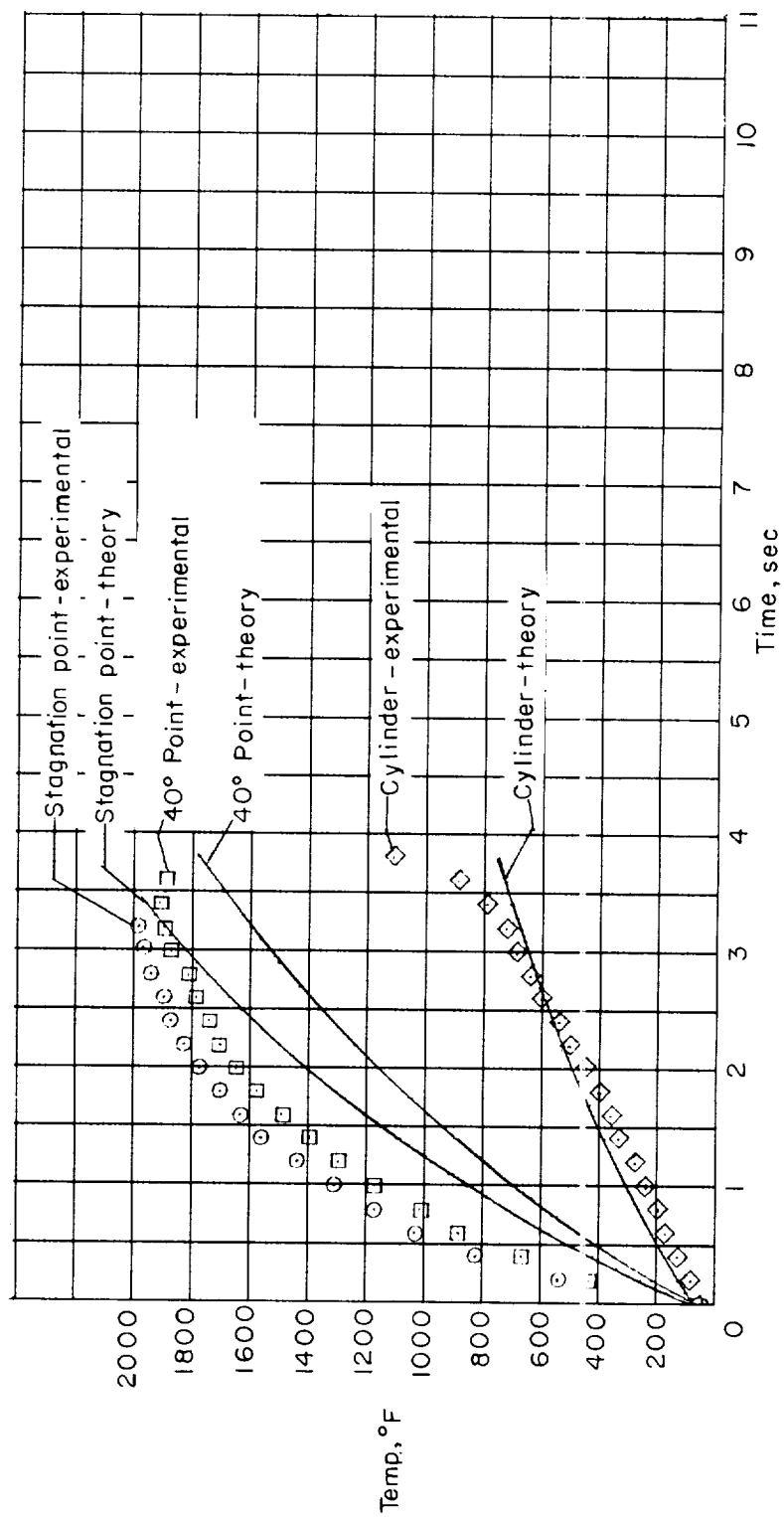
(a) $T_t = 2,000^\circ \text{F.}$

Figure 13.- Heating of the 3/4-inch-diameter hemispherical copper model. $p_t = 815$ psia.



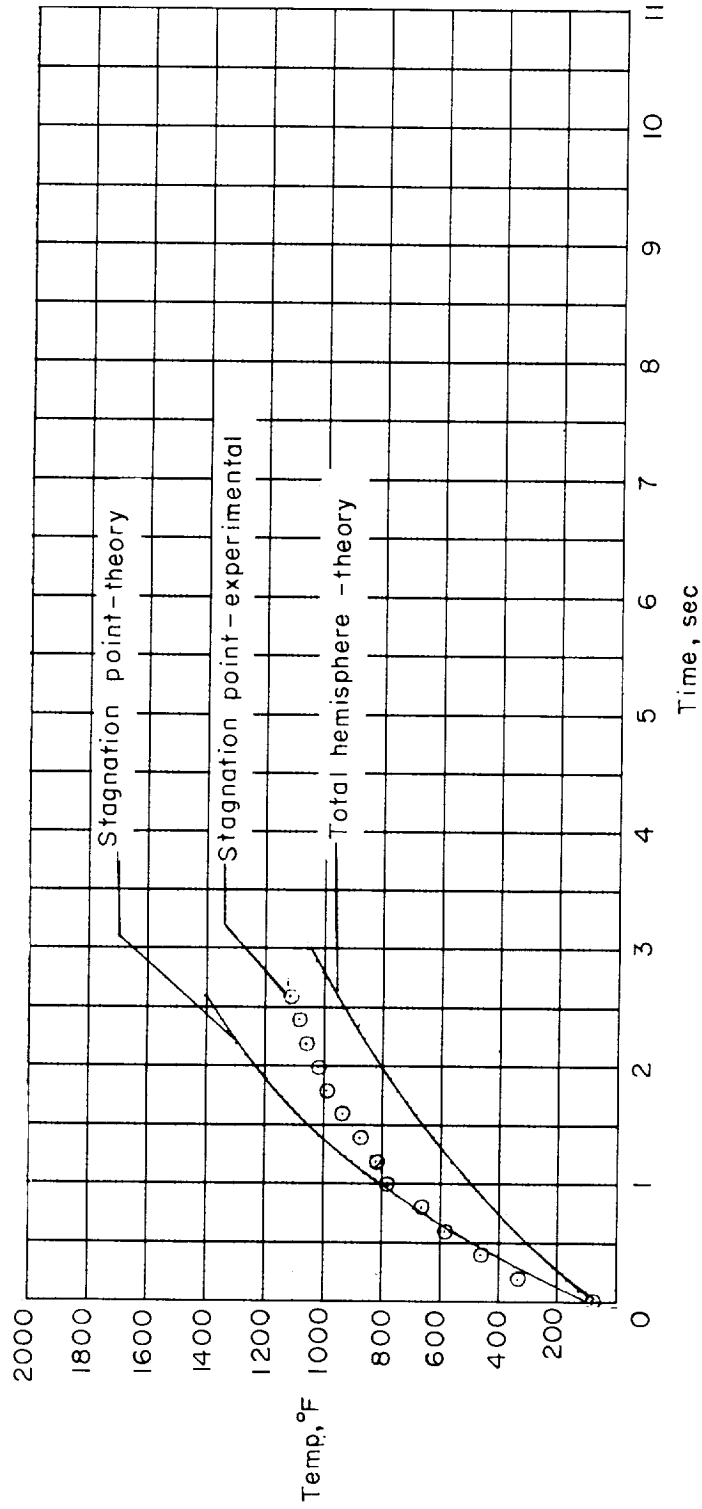
(b) $T_t = 2,900^\circ \text{F.}$

Figure 13.- Continued.



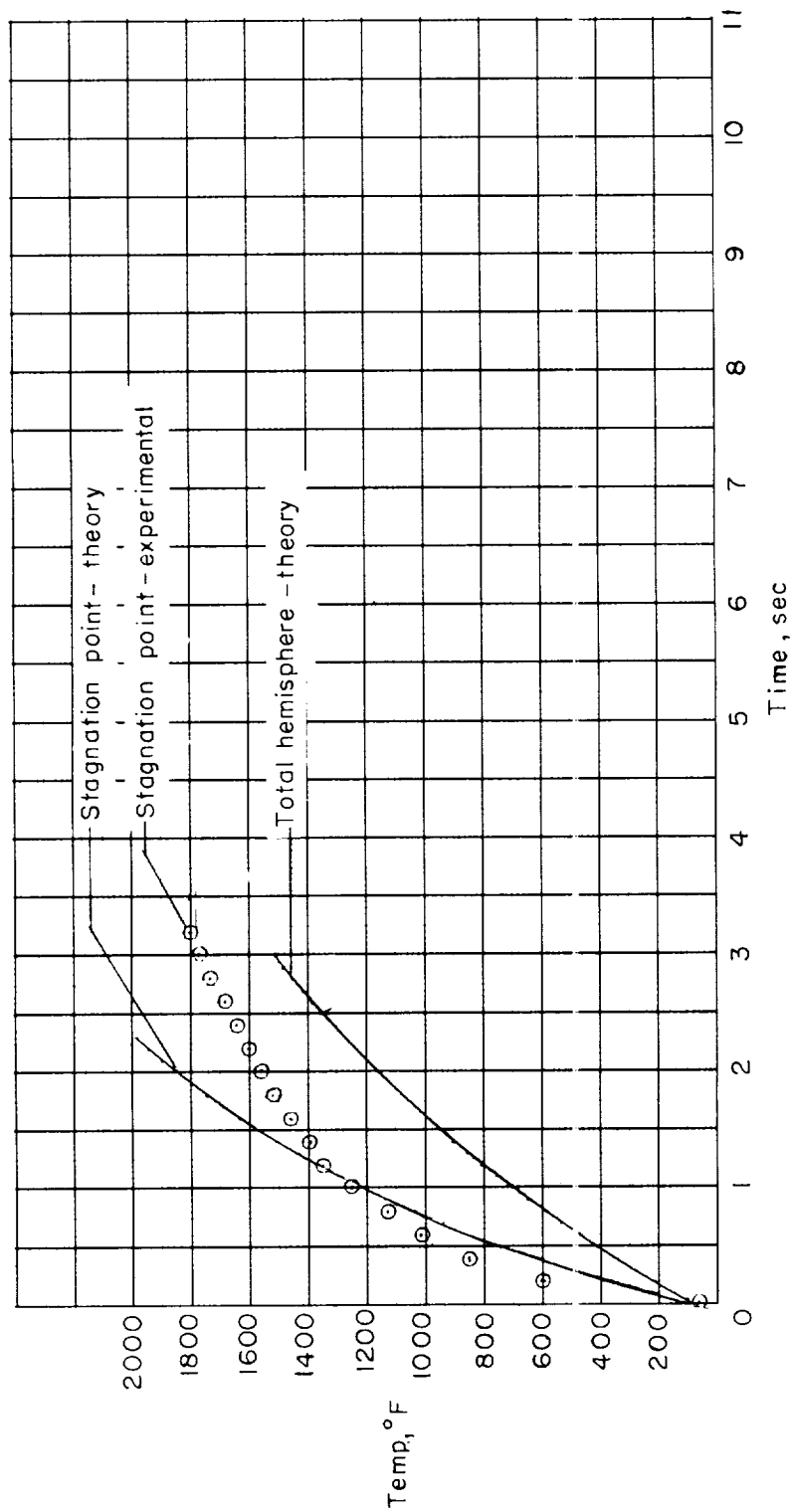
(c) $T_t = 3,540^\circ \text{ F.}$

Figure 13.- Concluded.



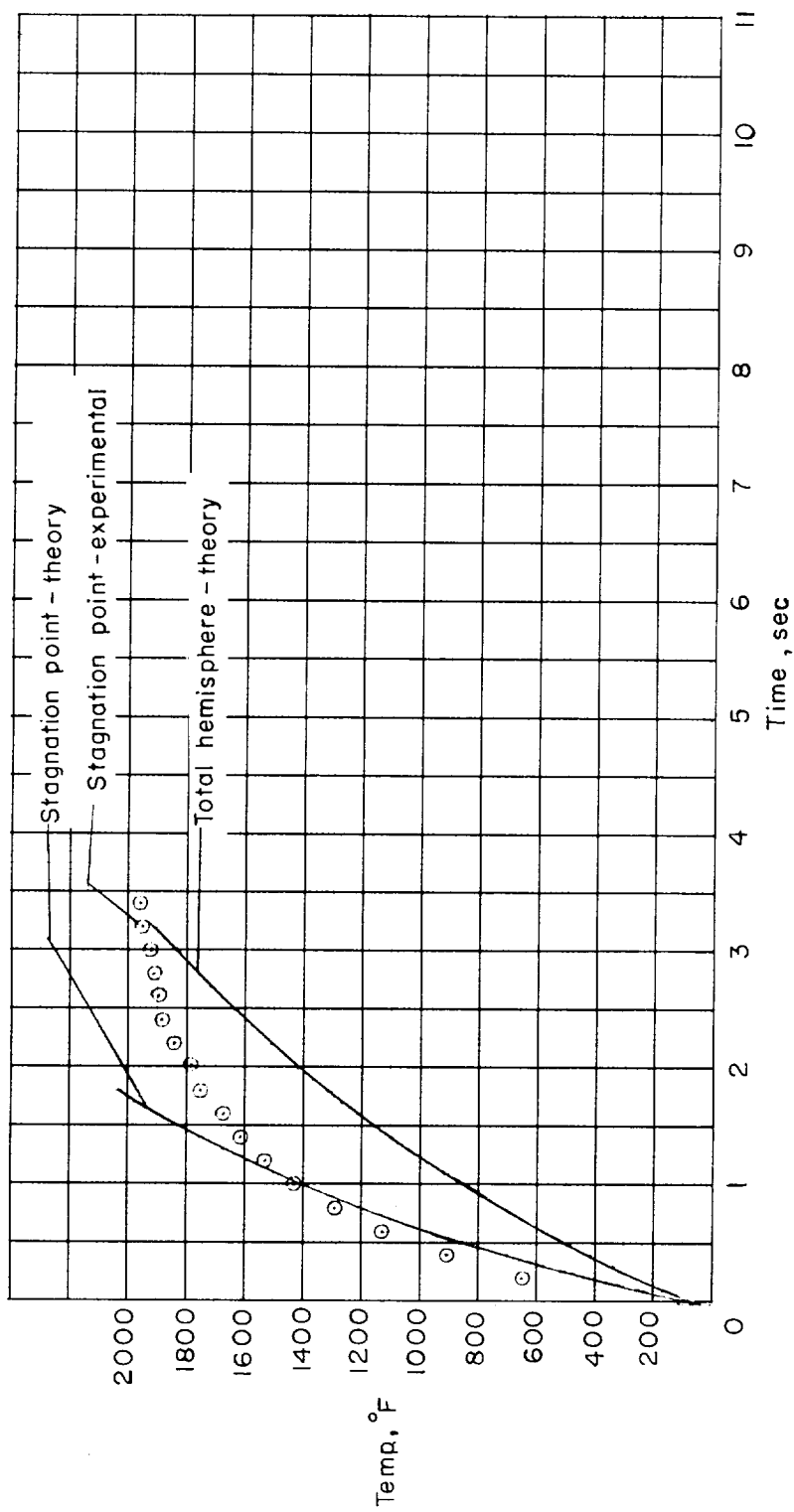
(a) $T_t = 2,000^\circ \text{F}$.

Figure 14.- Heating of the 3/8-inch-diameter hemispherical copper model. $p_t = 815 \text{ psia}$.



(b) $T_t = 3,040^\circ \text{F.}$

Figure 14.- Continued.



(c) $T_t = 3,560^\circ \text{ F.}$

Figure 14.- Concluded.

<p>NASA TM X-55 National Aeronautics and Space Administration. EXPERIMENTAL INVESTIGATION OF SEVERAL COPPER AND BERYLLIUM HEMISPHERICAL MODELS IN AIR AT STAGNATION TEMPERATURES OF 2,000° F TO 3,600° F. Otto F. Trout, Jr. September 1959. 41p. diagrs., photos. (NASA TECHNICAL MEMORANDUM X-55)</p> <p>(Title, Unclassified)</p> <p>The investigation was made in a Mach number 4 hot-air jet at Reynolds numbers of 1.88×10^6 to 2.93×10^6 to determine the resistance to heating of these materials when used as a heat sink. This investigation shows beryllium to be superior to copper in oxidation resistance, the amount of heat absorbed before melting, and resistance to ignition in air. A description of the testing apparatus is also presented.</p> <p>Copies obtainable from NASA, Washington</p>	<ol style="list-style-type: none"> 1. Flow, Supersonic (1.1.2.3) 2. Heat Transfer, Aerodynamic (1.1.4.2) 3. Materials (5) 4. Wind Tunnels (9.1.1) <p>I. Trout, Otto F., Jr. II. NASA TM X-55</p>	<ol style="list-style-type: none"> 1. Flow, Supersonic (1.1.2.3) 2. Heat Transfer, Aerodynamic (1.1.4.2) 3. Materials (5) 4. Wind Tunnels (9.1.1) <p>I. Trout, Otto F., Jr. II. NASA TM X-55</p>	<ol style="list-style-type: none"> 1. Flow, Supersonic (1.1.2.3) 2. Heat Transfer, Aerodynamic (1.1.4.2) 3. Materials (5) 4. Wind Tunnels (9.1.1) <p>I. Trout, Otto F., Jr. II. NASA TM X-55</p>
<p>NASA TM X-55 National Aeronautics and Space Administration. EXPERIMENTAL INVESTIGATION OF SEVERAL COPPER AND BERYLLIUM HEMISPHERICAL MODELS IN AIR AT STAGNATION TEMPERATURES OF 2,000° F TO 3,600° F. Otto F. Trout, Jr. September 1959. 41p. diagrs., photos. (NASA TECHNICAL MEMORANDUM X-55)</p> <p>(Title, Unclassified)</p> <p>The investigation was made in a Mach number 4 hot-air jet at Reynolds numbers of 1.88×10^6 to 2.93×10^6 to determine the resistance to heating of these materials when used as a heat sink. This investigation shows beryllium to be superior to copper in oxidation resistance, the amount of heat absorbed before melting, and resistance to ignition in air. A description of the testing apparatus is also presented.</p> <p>Copies obtainable from NASA, Washington</p>	<ol style="list-style-type: none"> 1. Flow, Supersonic (1.1.2.3) 2. Heat Transfer, Aerodynamic (1.1.4.2) 3. Materials (5) 4. Wind Tunnels (9.1.1) <p>I. Trout, Otto F., Jr. II. NASA TM X-55</p>	<ol style="list-style-type: none"> 1. Flow, Supersonic (1.1.2.3) 2. Heat Transfer, Aerodynamic (1.1.4.2) 3. Materials (5) 4. Wind Tunnels (9.1.1) <p>I. Trout, Otto F., Jr. II. NASA TM X-55</p>	<ol style="list-style-type: none"> 1. Flow, Supersonic (1.1.2.3) 2. Heat Transfer, Aerodynamic (1.1.4.2) 3. Materials (5) 4. Wind Tunnels (9.1.1) <p>I. Trout, Otto F., Jr. II. NASA TM X-55</p>

